TRAPPED PROTONS OF THE INNER RADIATION BELT *

by

R. Walker Fillius

A dissertation submitted in partial fulfillment of the requirements for the degree of Doctor of Philosophy in the Department of Physics and Astronomy in the Graduate College of the University of Iowa

June 1965

Chairman: Professor James A. Van Allen

*Research supported in part by the National Aeronautics and Space Administration under Contracts NAS5-1683 and NASr-116 and Grant NsG-538.

ACKNOWLEDGEMENTS

The author is indebted to Professor James A. Van Allen of the University of Iowa for his support and advice, and to Professor Carl E. McIlwain of the University of California San Diego who directed the building of the detectors while at the University of Iowa, and supervises the data reduction efforts which have been carried out at California. Dr. McIlwain's experience and advice have been indispensable. The author is grateful to Dr. Anthony Hassitt and Mrs. Anna De Vore both for the computer programs they contributed to the Relay library, and for their help in understanding the problems of computerized data reduction. Others who have contributed to the success of this experiment are Mr. Donald C. Enemark of the University of Iowa, Dr. John Valerio and Mr. Anil Davé of the University of California San Diego, and the many people at the RCA Astro-Electronics Division and the NASA Goddard Space Flight Center who built the satellite, operated it, and acquired and distributed the data. Mrs. Evelyn Robison made a special effort to type this manuscript, and it is a pleasure to acknowledge the many details that she took care of. For two and one-half years during this project the author held a NASA Traineeship at the State University of Iowa. The work was supported in part by NASA Contracts NAS5-1683 and NASr-116 and Grant NsG-538.

ABSTRACT

27386 over

Satellite Relay I has performed a thorough mapping of the energy spectrum and spatial distribution of protons in the inner zone. New intensity maps are presented in this paper for six energy ranges between 1.1 and 63 MeV as of January 1, 1963. With these six distributions and previously published intensities in two more ranges one can construct accurate energy spectra at arbitrarily selected locations throughout most of the inner zone. In any energy range the maximum intensity is found at the equator, and varies along a line of force near the equator as the third or fourth power of 1/B. There are fewer high energy than low energy protons, and they are found closer to the earth. Sample intensities are $j_\perp = 3.7 \times 10^6$ cm^{-2} sec^{-1} ster^{-1} from 1.1 to 14 MeV at L = 2.2 on the equator and $j_\perp = 1.6 \times 10^4$ cm^{-2} sec^{-1} ster^{-1} from 18.2 to 25 MeV at L = 1.6 on the equator. Comparison of Relay I data with other experiments are favorable and demonstrate the value of a comprehensive treatment. Neutron albedo sources, both cosmic ray and solar proton sources, are weaker than required by as

much as three orders of magnitude at 1 MeV. Adiabatic breakdown theories are in disagreement with the spatial dependence of the energy spectrum and cannot be controlling factors. Injection and diffusion of solar wind particles is a possible source, but more theoretical work is needed to clarify the expected results.

Author

TABLE OF CONTENTS

TABLE OF CONTENTS
(continued)

TABLE OF TABLES

I. INTRODUCTION

The inner zone of the Van Allen radiation belt is typified by stability of the spatial distribution and energy spectrum of the trapped radiation flux. In this region the earth's internally generated magnetic field greatly exceeds the externally generated fields produced by the ring current, hydromagnetic waves, or the solar wind interface. With the stable field dominating, we can expect preservation of the invariants of motion and long particle lifetimes.

The time stability of the radiation in this region permits a single satellite to obtain a complete survey of the spatial distribution before the distribution changes importantly. A complete survey at very high altitudes would require a veritable sea of satellites, measuring and telemetering their information simultaneously. When the distribution changes slowly with time, if it changes continuously, the change seen by each counter can be measured throughout space, and the intensity everywhere interpolated to some single time. Thus a complete map can be accumulated during a stable or slowly changing epoch, presenting the steady state distribution of each family of particles counted.

These spatial cross-sections are clearly important in efforts to find the sources, sinks, and transport mechanisms governing the particles. In the special case where there is no time change in the data, the distribution represents the equilibrium state; i.e., the solution of the transport equation with all spatial derivatives with respect to time set to zero. In the more general case the data represent the instantaneous energy and spatial distribution, or the solution of the transport equation for some instant of time. One of the accomplishments of a completely successful theory would be to predict this distribution. More practically, since no theory has met this test, the experimentally determined energy spectrums and spatial derivatives should provide the main terms of any equations formulated for this purpose.

Maps of the steady-state radiation fluxes are also of importance to engineers and scientists who need to know the radiation environment encountered by satellites and space-probes traversing this region. For instance, the feasibility of many satellite systems depends upon their ability to survive the radiation encountered in orbit. It has been shown [McIlwain et al., 1964] that the dosage received by a satellite is entirely

different for different types and energies of particles and is highly dependent upon the satellite orbit. Also it has been shown [Brown et al., 1963; McIlwain et al., 1964] that the degradation of solar cell power supplies and the effects observed by damage experiments are satisfactorily accounted for by the dosage on the satellite. The use of radiation flux maps will permit optimum design of satellites in arbitrary orbits.

Orbiting scientific experiments also must cope with the radiation environment, as it can produce undesired background effects. Peterson [1965] has shown how difficult it is to avoid such background. His low-energy gamma-ray experiment on OSO-1 included a Na I crystal surrounded by an anticoincidence shield to eliminate charged particle events. Although he did not count charged particles directly, he reports that neutrons were produced by the trapped protons bombarding the satellite materials, and some of these neutrons were captured by I^{127} in the crystal to form I^{128}, a radioactive species whose decays were observed following each pass through the inner zone. This effect is reminiscent of the "afterglow" seen by Vernov and Chudakov after each pass of their Sputnik III scintillator through the inner zone [Vernov and Chudakov, 1960]. The remarkable feature of the OSO-1 effect

is that the trapped radiation was anticipated and the detector designed so that all primary events were eliminated. Nevertheless, the unwanted background was produced by a two-step process, illustrating a difficulty that will be encountered by any low level counting system subjected to the trapped radiation.

Knowledge of the steady state distribution also enables one to monitor important changes in time. McIlwain [1964] observed a large impulsive change in the distribution of protons > 35 MeV which occurred during the major geomagnetic storm of September 1963. The spatial distribution, which was constant for months before and after the storm, underwent a large change during a period of hours. Besides demonstrating the clearcut connection with geomagnetic activity, this event allowed the complete recording of the distribution "before" and "after" --thus, a complete description of the change. Monitoring the slower, longer-period behavior as well will help to identify the causes of the redistribution of geomagnetically trapped particles.

II. PRESENTATION OF THE DATA

1. Instrumentation

This paper concentrates on two of the four State University of Iowa-University of California San Diego instruments on Relay I. Using pulse height discrimination, these detectors generate six energy bands of data on the trapped proton fluxes. Table I summarizes their characteristics and Table II lists the nominal orbital parameters of Relay I. Previous reports have described the design and calibration of those instruments quite thoroughly [Fillius, 1963; Fillius and McIlwain, 1962; McIlwain et al., 1964]. These references can be consulted for a more detailed review of the instrumentation.

The satellite data system is quite reliable. The output of each detector is digital, with digital telemetry and data handling. The discriminators and scalers are linear for the counting rates experienced by these detectors and a redundant readout in the telemetry frame guards against transmission errors.

The major source of instrumental error is the temperature dependence of the discrimination levels, which change by 20% in the operating temperature range of -5 to + 30 °C. For the

steepest energy spectrum encountered, different temperatures can cause up to a 50% change in the counting rate. A correction has been applied to the data presented here, using the temperature coefficients determined in the laboratory and the temperatures recorded in flight. For the spectrum observed by the shifted discrimination levels, an interpolation or extrapolation is made to the calibrated levels to determine the counting rate that would have been observed in the quoted energy range. The mathematical form of this correction is given in the Appendix, and an example is shown in Figure 1, frames 1, 2, and 4. The energy spectrum is very steep in this example and the change is substantial, although, it appears, slightly undercorrected. Rarely does the temperature correction to the B detector data amount to more than 40%, and generally it is less than 20%. That to the C detector data is rarely more than 30% and generally less than 15%. The main effect of the temperature correction is to reduce the scatter in the data points. It may be noted that previously published data [McIlwain et al., 1964; Fillius and McIlwain, 1964] does not include the temperature correction to the detector C data.

A more serious change occurred in the detector B data and is attributable to radiation incurred gain loss. From laboratory experience one expects that a semiconductor detector will deteriorate after receiving a high dose of radiation [Dearnally, 1963]. Decreased resolution, increased resistivity, and, eventually, decreased gain are the effects to be expected. Because resolution is not critical to the Relay three-channel spectrometer, the first effect was not evident.

Increased resistivity manifested itself after a few months in the form of a higher counting rate in a background channel. The discrimination level for this channel had been set above the maximum energy loss for protons entering the aperture, so that the channel would count only background particles coming from the side. However, as the depth of the sensitive volume is proportional to the square root of the resistivity and the maximum energy loss is proportional to the depth, more and more foreground particles were able to trigger this discriminator. This effect is unimportant to our results, as the background channel was only a performance check for the detector, and the data from the other channels are projected to January 1, before the change became substantial.

The gain started to decrease after 100 days in orbit, when the integrated dose on the detector had reached about 10^{12} particles/cm^2. Between April 10 and May 10, 1963 the gain decreased from 1 to 1/2, the counting rate dropping by as much as a factor of 10, and after May 10 the counting rate continued to drop, exhibiting occasional bursts of noise, until the detector stopped counting in June. Previously published analyses of detector B data have included only data taken before the change in April. However, because of a satellite power supply failure, the data coverage in this period was poor, good coverage not being obtained until April. Consequently the previous analyses had to be done by hand in order to get the most out of the somewhat sketchy data.

For the present report data taken between April 10 and May 10 have been recovered by a correction, similar to the temperature correction, but using an empirically derived curve of gain vs time. Illustrated in Figure 1, frames 2, 3, and 5, the correction increases from no change to a factor of ten change at the highest. With the augmented data the coverage is more complete, and data analysis can be done by computer. The justification of the radiation-damage correction lies in the

curve of gain vs time. First of all it is distinctly more probable that the loss of counts in detector B was due to this predictable effect of radiation damage than that it was due to the complete disappearance of low energy protons from the inner belt. Furthermore, the time stability of these particles has been confirmed by all of the comparisons in chapter III of this paper, by an identical detector on Relay II, and by the data received from Relay I up to the period in question. The alteration of a single parameter, detector gain, was sufficient to restore the data in question to values that agree with the previous distribution, and the restoration was successful over all space for three separate energy ranges. For these reasons the radiation-damage correction is felt to be well-founded, and the new distributions are considered the most accurate obtainable.

2. Data Reduction

The complex data analysis program used for this survey was developed by McIlwain [1963] for Explorer XV data. The method will be reviewed here as it has been applied to Relay I.

The raw satellite data consists of counting rates for the several detectors versus time. The position of the satellite as a function of time is provided by NASA and added to the data.

Position is calculated in magnetic coordinates, or B, L space [McIlwain, 1961]. From this is obtained the counting rates versus B and L. Next a computer program interpolates the data to selected magnetic shells (L = 2.0, 2.05, 2.1, etc.) wherever the orbit crosses them and the data are usable. The interpolated data are grouped according to L value and sorted in order of B. With adequate data, one can then plot the counting rates as a function of B for any selected L. Usually there is a strong B dependence.

As each crossing of a magnetic shell occurs at a different time, the time dependence has so far been left out. For proton data it is typically small. When the time variation is regular, and not a function of B, one can fit the flux on a line of force with the function

$$\begin{aligned} \ln_e \Phi &= \ln_e (1/G) + A_1 + A_2 t \\ &+ A_3 (B/B_o) + A_4 (B/B_o)^2 + \ldots \\ &+ A_n (B/B_o)^{n-2} \end{aligned} \qquad (1)$$

where

$B_o = .3116/L^3$ is the value of the magnetic field at the equator for that L;

$3 \leq n \leq 8$ is selected by the computer or by the programmer for the best fit;

G is the geometric factor in cm^2-sr for the detector.

One sees that the given function can produce a strong B dependence and a weak t dependence as required. Satisfactory coefficients A_1, -- , A_N have been obtained on a grid of L values for each of the six data channels of this survey.

During a stable or slowly changing epoch a counting rate at time t can be projected to a reference time t ref by multiplying by exp $(A_2 (t - t\ ref))$. The result is the intensity that would presumably have been measured at the reference time. The steady-state distributions given in this paper represent such presumed intensities, projected to January 1, 1963. Data in the three ranges of detector B were taken during the interval from December 14, 1962 to May 10, 1963; in the three ranges of detector C, from December 14, 1962 to September 22, 1963.

3. Proton Fluxes

Figures 2 through 7 illustrate the flux as a function of B for the six energy ranges of detectors B and C. Figure 8 shows

the sum of the detector C channels, or the flux of protons from 18.2 to 63 MeV. The points represent the individual measurements projected to January 1, 1963, and the line is the analytical fit according to equation (1). These figures include only six or seven lines of force. Relay I data have been analyzed in these seven energy bands on up to 28 lines of force. Because its bulk is too great to be included in the present paper, the complete set of data is available in a supplementary report [Fillius and McIlwain, 1965]. The supplementary report contains figures for all of the lines of force and tables of the fitting coefficients in equation (1). Offering no interpretation, the report is intended as a reference manual for proton fluxes, and as a detailed presentation of Relay I data.

Inspection of these figures shows that between L = 1.5 and 2.2 the intensity within about 30° to 45° of the equator can be approximated by a power law

$$j = j_Q \ (B/B_o)^{-n} \ .$$

For the lowest energy range (1.1 to 14 MeV) the slope, n, is typically 3.5 to 4, and for the highest energy range (35 to 63 MeV) the slope is about 3. As one goes away from the equator the

slope decreases, the intensity being a less critical function of B, until the mirror points start to fall in the dense atmosphere. Here the intensity drops suddenly, as particles mirroring in the dense atmosphere quickly lose their energy in collisions and recombine to become untrapped neutral atoms.

Using the analytical fits of equation (1) as a first simplification, one can condense the data further by means of contour maps in B, L space. A complete set of contours displays all of the information from a given channel. Figures 9 through 15 exhibit the flux of protons in seven energy ranges as seen by Relay I on January 1, 1963. Six energy ranges are independent and one is redundant. As there are ten contours per decade on these maps, the step size is one db, or about 25%. The error in the data is ususally less than this.

In studying the contour maps it may help to remember that the previous plots, Figures 2 through 8, are cross-sections of the contour maps along the appropriate lines of force. The intensity of protons which mirror at a given B and L can be read at the point B, L on the maps. These particles remain on the same L shell as they drift around the earth and spend their time between the equator and their mirror points, B, in each

hemisphere. The high intensity contours lie near the equator, the highest intensity observed being 3.7×10^6 protons cm^{-2} sec^{-1} $ster^{-1}$ from 1.1 to 14 MeV at L = 2.2. The peak intensity in this energy range evidently lies above the Relay I apogee, as the highest contour is not closed and the intensity still rises going outward on an equatorial profile. The atmosphere is evident at high values of B where the close spacing of the contours indicates a steep intensity gradient. This is the underside of the radiation belt where the lines of force enter the dense atmosphere.

Although the perigee of the Relay I orbit is 1.2 earth radii, not enough data were acquired below L = 1.5 to permit plotting low energy proton intensities on these lines of force. Additionally, the high electron fluxes at low L values contaminated the highest energy channels of detector C, so that no data is displayed for 35 to 63 MeV protons below L = 1.8 and for 25 to 35 MeV protons below L = 1.6. With these exceptions, however, the coverage over the orbit is complete, and the Relay I data maps provide a broad view of the inner zone proton distribution.

4. Proton Energy Spectra

The six energy bands of detectors B and C can be augmented by two more ranges obtained by detectors A and D. Table III summarizes the properties of these detectors. After converting the detector A measurements from omnidirectional to directional flux, one has eight points with which to construct the energy spectrum of directional protons. The eight energy ranges are listed below:

Detector B	1.1	to	14	MeV	directional
Detector B	1.6	to	7.1	MeV	directional
Detector B	2.25	to	4.7	MeV	directional
Detector D	> 5.2			MeV	directional
Detector C	18.2	to	25	MeV	directional
Detector C	25	to	35	MeV	directional
Detector C	35	to	63	MeV	directional
Detector A	> 34			MeV	converted from omni-directional to directional

It is easiest to make an integral spectrum, so that the fluxes determined by detector A and detector D can be plotted immediately. A small adjustment is then made to the 34 MeV

point to give the flux above 35 MeV. This adjustment is determined by the steepness of the spectrum measured by the upper two ranges of detector C. Assuming a power law energy spectrum,

$$N\ (>E) \;=\; K\,E^{-n} \tag{2}$$

the correction formula is

$$\frac{dN}{N} \;=\; -n\ \frac{dE}{E} \;=\; -\ .03\ n \tag{3}$$

and n comes from the formula

$$\frac{N\ (35 \text{ to } 63)}{N\ (25 \text{ to } 63)} \;=\; \frac{35^{-n} - 63^{-n}}{25^{-n} - 63^{-n}} \quad . \tag{4}$$

As n is typically 3 or less, the correction is about 10%. For such a small correction the assumed spectral form is unimportant and does not prejudice the data.

Now one can add the flux of protons from 25 to 35 MeV to the total flux above 35 MeV to get the total above 25. Again adding the flux from 18.2 to 25, one has the total above 18.2. An interpolation between 18.2 and 5.2 MeV gives the flux above 14 MeV. If this is added to the 1.1 to 14 MeV range, one has the flux above 1.1 MeV. Similar interpolations to 7.1 and 4.7 MeV

and additions to the appropriate detector B ranges gives the fluxes above 1.6 and 2.25 MeV. The spectrum is completed at the high end either by extending a power law to 63 MeV or by subtracting the 35 to 63 MeV flux from the > 35 MeV value. Although the former method introduces an assumption of the spectral form, it is generally safer than the latter method, which depends upon a small difference between two large numbers.

Figures 16 and 17 taken from McIlwain et al. [1964] and McIlwain [1964] give the fluxes above 5.2 and 35 MeV measured by detectors D and A. Complete spectra can now be constructed, using the data maps in this paper, over much of the inner zone.

III. OTHER MEASUREMENTS IN THE INNER ZONE

1. History

Measurements of inner zone protons have exhibited increasing precision since the Geiger tubes on Explorer I and III discovered the trapped radiation [Van Allen, 1959]. The instruments of Explorer IV mapped the first intensity contours, but did not positively identify the type of radiation they were measuring (protons, electrons, bremsstrahlung, or heavier nuclei) [McIlwain, 1961]. Nuclear emulsion packs flown and recovered on high altitude rockets disclosed proton tracks which identified the penetrating radiation of the inner zone [Freden, White, 1959; Naugle and Kniffen, 1962]. Intensities and energy spectra were also obtained by the emulsions, but their time and spatial revolution was poor and the extent of coverage was, of course, very limited. Proton detectors of improved performance and energy resolution have been flown into this region on rockets [Bame et al., 1963] and satellites [Davis and Williamson, 1963; Bostrom et al., 1961; McIlwain, 1963; Brown and Gabbe; Imhof and Smith, 1964; Freden and Paulikas, 1964; Fillius and McIlwain, 1964; Freden et al., 1965; Krimigis and Van Allen, 1965], increasing the accuracy of our knowledge of this trapped radiation.

The remainder of this chapter will be devoted to comparison of the measurements of other experimenters with those of Relay I. It will become evident that a wide range of detectors, from nuclear emulsions to zinc sulphide scintillators, have obtained reproducible results, and that these diverse experiments all fit the space and energy distributions found by Relay.

2. Comparison with NERV

One of the important emulsion experiments was a nuclear emulsion recovery vehicle (NERV) rocketed through the inner zone on September 19, 1960. The emulsion was rotated past a window in flight, and the recovered film was scanned at five different points which passed under the window at the five locations given below in B, L coordinates [Naugle and Kniffen, 1962; Naugle and Kniffen, 1963].

Location	B	L
A	0.231	1.79
B	0.198	1.72
C	0.196	1.64
D	0.209	1.54
E	0.223	1.47

The spectra for these points established that there was a soft component of the proton spectrum which disappeared at low L values. This trend was qualitatively confirmed by previously published Relay I results [Fillius and McIlwain, 1964]. With the method for constructing spectra explained in the previous chapter, and using the data presented in this paper, one can make a quantitative comparison between NERV and Relay I at point A. The high energy proton detectors on Relay have a high electron background at the other points and comparison there is not possible. Figure 18 demonstrates the agreement. The time gap between measurements is 2 1/2 years, yet there is no change beyond the accuracy of the measurements.

3. Comparison with Bame, Conner, Hill, and Holly [1963]

On October 4, 1960 another rocket carried a two-crystal scintillation spectrometer into the inner zone to measure the proton spectrum. The result reported by Bame, Conner, Hill, and Holly is an average for protons having pitch angles between 60° and 90° at L = 2.495 and B = .069. For $1.02 \leq E \leq 2.24$ MeV,

$$j(E) = 2.0 \times 10^{6} E^{-5.2} \text{ protons/cm}^2 \text{ sec ster MeV}$$

and for $2.24 \leq E \leq 7.3$ MeV

$$j(E) = 0.71 \times 10^{6} E^{-3.9} \text{ protons/cm}^2 \text{ sec ster MeV.}$$

The number above 7.3 MeV is consistent with an extrapolation of the latter spectrum to infinity.

For comparison with a Relay I spectrum constructed for this point, the spectrum of Bame et al. (B, C H^2) has been integrated and plotted in Figure 19. The Relay I data are also shown. Once again the comparison is pleasing. For $E > 2.25$ MeV, there is no meaningful difference. Below 2.25 MeV the B, C, H^2 spectrum is softer, so that the earlier experiment sees almost three times as many protons above 1.1 MeV as does Relay. This may correspond to a real time variation. If this is the case the difference could be generated merely by turning off the source and letting the protons lose energy in the residual atmosphere during the time interval between measurements. Other mechanisms could generate this difference also, but it is clear that a sophisticated process is not needed.

4. Comparison with Injun I [Pieper, Bostrom, and Zmuda]

The satellite Injun I carried a solid state detector which counted protons from 1 to 15 MeV, almost the same range as Relay, and this counter obtained trapped proton data in its circular, 1000 km orbit from June, 1961 until December. Bostrom, Zmuda, and Pieper have published a comparison of the fluxes measured by Injun I with the preliminary Relay I contours published by McIlwain et al. [1964]. This comparison is repeated in Figure 20, where the final Relay I contours presented in this paper have been added, as well as some reference lines of constant altitude. Although the preliminary Relay I contours were not guaranteed to be less than a factor of two in error, they are not significantly different from the final ones, which should be accurate to 25%. The final contours were not extended below $L = 1.5$ because there are too few data in that region to give better than factor-of-two accuracy.

As noted by Bostrom et al., the Injun data are in good agreement with Relay in the region $1.6 \leq L \leq 1.9$, and in the region $1.9 \leq L \leq 2.5$, $.22 \leq B \leq 0.25$, the Injun data are a reasonable extrapolation of Relay.

Below L = 1.5 the Injun data are not a good extrapolation of the Relay contours, and is up to a factor of 8 less than the preliminary Relay contour through that region. Although this is an indication that the particle fluxes have changed in this region, it seems inadvisable to base a firm conclusion on so little data. Generally speaking, the comparison with Injun I data indicates a high degree of stability of the trapped radiation in this region.

5. Comparison with Freden, Blake, and Paulikas

The satellite 1964-45A was launched in August, 1964 with a complement of proton detectors which monitor six energy ranges from 6 to > 110 MeV. A set of spectra from the first two weeks in orbit has been distributed by Freden, Blake, and Paulikas [Freden et al., 1965] and four of these spectra are from points where Relay I data can be assembled. As the Freden, Blake, and Paulikas (F, B, P) results are given in omnidirectional, differential spectra, and the Relay I fluxes are best expressed as directional, integral spectra, there is some difficulty in matching the curves. This has been done on the middle ground by comparing omnidirectional, integral spectra. Conversion of the

F, B, P curves from differential to integral spectra is straightforward, using the given properties of the detectors to convert the differential data to direct fluxes and then building integral spectra in a fashion analogous to that used for Relay. To convert the Relay I fluxes to omnidirectional, recourse was made to curves of intensity versus B along a line of force (e.g., Figures 2-8). The omnidirectional intensity was integrated from the position of the comparison, B, down to the atmosphere at B_{MAX}:

$$J(B) = 2\pi \int_0^{\infty} j(\alpha)\, d\alpha \sin\alpha$$

$$= 2\pi \int_0^{B_{MAX}/B} \left(\frac{j(xB)}{x^2 \quad 1 - x^{-1}} \right)_{dx} . \qquad (5)$$

Error bars have not been put on the resulting Relay fluxes because of the difficulty in tracing them through the integral.

Figure 21 shows the comparison between the spectra. Clearly the agreement is excellent.

6. Comparison with BTL

In addition to the SUI-UCSD detectors listed in Tables I and II, Relay I carried two detectors built and calibrated by the group at the Bell Telephone Laboratories. An unpublished report

on Relay I results [Brown et al., 1964] gives flux contours for protons in two energy ranges: 2.5 to 3.8 MeV, and 5.0 to 8.6 MeV. Because the energy thresholds do not coincide with those of the SUI-UCSD counters, comparison must be made by constructing an SUI-UCSD integral spectrum, and interpolating to read the flux values at the BTL thresholds. It is convenient to do this at the equator, using a previously published [Fillius and McIlwain, 1964] set of SUI-UCSD spectra, and reading the BTL fluxes from their contour plots. The resulting equatorial profiles are shown in Figure 22.

Agreement is tolerable in the 2.5 to 3.8 MeV range, but in the 5.0 to 8.6 MeV range the BTL fluxes are consistently about 50% higher than the SUI-UCSD values. As a 15% error is quoted for the BTL contours, and the SUI-UCSD values are given about a 30% uncertainty, this is outside the error bars. In this case the detectors are on the same satellite, and no time variations can be considered. Three possible explanations are offered:

(1) The error bars on the SUI-UCSD points are uncertain, as they are taken from the difference of two large numbers. The errors shown were assigned according to the formula

$$(x \pm \Delta x) - (y \pm \Delta y)$$

$$= (x - y) \pm \sqrt{\Delta x^2 + \Delta y^2} \quad . \qquad (6)$$

The errors x and y are probably not randomly related, however, and if they are oppositely directed, the error bars should be much larger. In this case the discrepancy is unreal.

(2) One of the SUI-UCSD or BTL detectors has a different energy threshold from that quoted. A slight difference in threshold could make a large difference in flux.

(3) The proton spectrum does not vary smoothly between 5.2 and 18.2 MeV, but drops very fast from 5 to 8.6 MeV and then levels off before dropping again above 18.2 MeV. In fact, the SUI-UCSD value for the total flux above 5.2 MeV falls within the BTL limits for the energy range 5.0 to 8.6. As the SUI-UCSD fluxes were read between 5.2 and 18.2 MeV by assuming a simpler spectrum, the interpolated values would contain this error. In this case also, the discrepancy would be unreal.

7. Comparison with Explorer XV

Explorer XV carried an omnidirectional proton counter almost identical to detector A on Relay I. McIlwain [1963] has published

data from this detector in the 40 to 110-MeV range, and Fillius and McIlwain [1964] have published a comparison with Relay I in the form of equatorial profiles (see Figure 23). In this figure one of the detector C channels goes through a minimum at 1.9 R_E whereas the others do not. Since the data handling for these three channels is identical, it is clear that the minimum is tied to the different energy sensitivity of that data channel, and is not an artifact of data reduction.

8. Comparison with Davis's Measurements

One of the most important bodies of data on low energy trapped protons is that of L. R. Davis and his group at Goddard Space Flight Center [Davis et al., 1962; Davis, 1965]. Their Ion-Electron detector has an upper proton cutoff at about 10 MeV and lower thresholds at 98, 134, 168, 268, 498, 988, and 1688 keV. The upper two ranges compare closely with two of the ranges of detector B (see Table I), and it is of interest to compare the Relay I results with Davis's data from satellites Explorer XII, XIV, and XV. Figure 24 makes this comparison by spotting some of Davis's data over a Relay contour map. Davis's points are taken from a preliminary, unpublished table "HSi" [Davis, 1965],

and the block around each point is the projection in B, L space of the range of pitch angles over which the Davis value was averaged. Cursory inspection reveals agreement within a factor of two everywhere. Detailed examination discloses two regions where there is apparent disagreement.

(1) At low L values near the equator Davis's values are lower than Relay I.

(2) At high L values ($L \geq 3.5$), Davis's average is higher than Relay I.

The comparison at low L values near the equator will be in better (perhaps full) agreement after a proper spin-average correction is made to the preliminary HSi data shown here [Davis, 1965]. The difference at high L values can be explained on the basis of the different energy thresholds of the detectors. Representing a soft energy spectrum as a power law, one expects the ratio of the measurement to be

$$\frac{N(>.988)}{N(>1.1)} = \left(\frac{.988}{1.1}\right)^{-n} = 10^{.0458n} \quad . \tag{7}$$

At L = 3.5, n is about 5, and the Davis flux is expected to be about $10^{.23}$ higher, as observed. Below L = 2.5 ($n \approx 2$) the correction is unimportant and the agreement is not impaired.

The comparison with Davis's measurements, then is quite favorable.

9. Summary of Comparisons

In this chapter seven other experiments in the inner zone have been compared with the Relay I measurements. The results of the comparison are as follows:

(1) There is no more than minor disagreement between the experiments.

(2) Measurements from September, 1960 through August, 1964 exhibit no changes beyond the accuracy of the experiments. The time stability implied by this fact will be discussed in the next chapter.

(3) Given eight Relay I intensity maps, one can construct accurate energy spectra at arbitrarily selected locations throughout most of the inner zone.

IV. APPLICATION TO THE PHYSICS OF THE INNER ZONE

It is best to acknowledge that there is no adequately developed theory to account for the fluxes measured by Relay I. A full review of theoretical work on proton trapping is not in order here, but several studies will be presented for the application of our data.

1. Time Changes in the Proton Flux

It is a notable result of Chapter III that there is no significant difference between the fluxes seen in September 1960 by NERV, in January 1963 by Relay I, and in August 1964 by satellite 1964-45A. Comparing the flux and spectrum above 18.2 MeV, one can state that there is no more than a 40% difference between September 1960 and January 1963 and no more than 40% between January 1963 and August 1964 at the respective points of comparison. It is not clear, however, that these fluxes remained the same continuously during the entire four year span.

Small drifts did occur in some of the Relay I data over the period December 1962 to September 1963, but their interpretation is ambiguous. These drifts could be due either to genuine changes

in the proton fluxes or to gradual changes in the detector characteristics. This question will be resolved when a thorough study is finished using Relay II data to recalibrate the Relay I detectors as of January 1964. In the case that there is a drift in the detector characteristics, it should be clear that it does not affect the distributions presented in Chapter II, since these curves represent the projection of the data back to the time of launch, i.e., to the counting rates that would have been observed before the calibrations changed. In any case, the rate of drift is small, corresponding in many cases to a change over the period of observation that is less than the scatter in the data.

That the proton fluxes do change has been recorded by Pizzella, McIlwain, and Van Allen [1962] interpreting data from the 302 Geiger tube on Explorer VII, and by McIlwain [1964] analyzing detector A data from Relay I. All of these changes have been associated with geomagnetic disturbances. For instance, the change reported by McIlwain was the only major event that occurred during the Relay I lifetime, and it coincided with the magnetic storm of September 1963, when the index A_p

reached 600 γ. The Relay I detector B and C data in Chapter II was taken from launch until September, and during this period A_p was never higher than 264 γ. Significantly, this level was exceeded in twelve storms during the Explorer VII study, and 600 γ was exceeded in three storms. It is not surprising then, that Explorer VII recorded more activity. After the September 1963 storm detector C shows a change similar to detector A, but the data have been sparse and need careful interpretation in light of possible calibration drifts. Detector B was quite dead by this time, and yields no information. Therefore this change has not been analyzed in the present paper, which is intended primarily to present the spatial distribution at one moment of time.

2. CRAND

Before the identification of the penetrating radiation of the inner zone, it was suggested [Singer, 1959] that these particles were protons from the decay of neutrons produced at the top of the atmosphere by cosmic rays. The cosmic ray albedo neutron decay theory (CRAND) had some success in accounting for the early crude measurements and still gives plausible

results at low altitudes for > 40 MeV protons [Valerio, 1964]. For the 1 MeV protons in the Relay I orbit, however, a source is needed which is stronger by two or three orders of magnitude. To demonstrate this fact one can calculate the source strength needed to sustain the flux measured by Relay I at some point in space and compare this with the source strength provided by CRAND. Ray [1960] has solved the proton transport equation for equilibrium between a neutron injection source and atmospheric losses:

$$j(E) = \bar{\rho}^{-1} \left(- dE/dx \right)^{-1} \int_{E}^{\infty} \overline{S(E)}\, dE \qquad (8)$$

where $j(E)$ is the proton flux, in p sec^{-1} MeV^{-1} $ster^{-1}$ cm^{-2}.

$\bar{\rho}$ is the average atmosphere over a longitudinal drift period, in gm cm^{-3}.

dE/dx is the energy loss rate for a proton in the atmosphere, in MeV gm^{-1} cm^{-2} .

$\overline{S(E)}$ is the injection rate for protons of energy E averaged over a longitudinal period, in protons sec^{-1} MeV^{-1} $ster^{-1}$ cm^{-3}.

Consider 1 MeV particles mirroring at the equator at L = 2.1. Using Relay I data for $j(E)$, a computer program by Hassitt [1965] for $\bar{\rho}$, and a handbook value for dE/dx, one gets

$$j(1) = 2.1 \times 10^{6} \text{ protons cm}^{-2} \text{ sec}^{-1} \text{ ster}^{-1} \text{ MeV}^{-1}$$

$$\bar{\rho} = 3.8 \times 10^{-21} \text{ gm cm}^{-3}$$

$$dE/dx = -250 \text{ MeV gm}^{-1} \text{ cm}^{2}$$

$$\int_{1}^{\infty} \overline{S(E)}\, dE = 2.0 \times 10^{-12} \text{ protons cm}^{-3} \text{ ster}^{-1} \text{ sec}^{-1} .$$

This is the source strength required by trapped proton observations.

Now consider the mechanics of albedo neutron injection. By an argument of Singer and Lenchek [1962] the injection coefficient into a given trapped orbit is proportional to the fraction of that orbit during which the particle velocity vector scans the earth. This represents the fact that the neutron is traveling on a straight line away from the earth at the instant of decay, but the decay proton becomes averaged over all phases in its trapped orbit including those in which injection is not possible. For equatorial particles at L = R this dilution factor, g, is given by

$$g = \frac{1}{\pi} \sin^{-1}(1/R) \quad . \tag{9}$$

The neutron leakage flux at a point in space can be calculated on the basis of the papers of Hess, Canfield, and Lingenfelter [1961] and Lingenfelter [1963]. We will use the following notation:

$J(\lambda, E)$ = the flux of neutrons of energy E leaking out of the top of the atmosphere at latitude λ, expressed in neutrons $cm^{-2}\ sec^{-1}\ MeV^{-1}$.

$J(\lambda, E, \zeta)$ = the directional neutron flux at the top of the atmosphere with energy E, at latitude λ, and with zenith angle ζ, expressed in neutrons $cm^{-2}\ sec^{-1}\ MeV^{-1}\ ster^{-1}$.

$J(R, \lambda, E, \alpha)$ = the directional neutron flux at a position in space given by radial distance R and latitude λ, with energy E, and angle α with respect to the local magnetic field vector, expressed in neutrons $cm^{-2}\ sec^{-1}\ MeV^{-1}\ ster^{-1}$.

Hess et al. showed that the angular distribution of neutrons escaping from the top of the atmosphere was expressed by the factor

$$\cos\zeta + \frac{3\cos^2\zeta}{2.13} \quad .$$

Throwing away the first term, they approximated this simply by $\cos^2 \zeta$, and gave the angular distribution as

$$J(\lambda, E, \zeta) = \frac{3}{2\pi} \cos^{-2} \zeta \; J(\lambda, E) \tag{10}$$

where $\frac{3}{2\pi}$ is a normalization constant to assure that

$$2\pi \int_0^{\pi/2} J(\lambda, E, \zeta) \sin \zeta \; d\zeta = J(\lambda, E) . \tag{11}$$

It is almost an equally good approximation to throw away the second term and write

$$J(\lambda, E, \zeta) = \frac{1}{\pi} \cos \zeta \; J(\lambda, E) . \tag{12}$$

This form has the advantage of simplifying the solution of equation (13).

The directional neutron flux at radial distance R and latitude 0°, with energy E and angle 90° to the local magnetic field vector, is given by

$$J\,(R,\ 0°,\ E,\ 90°) \;=\; \lim_{\epsilon \to 0} \frac{\int_{\phi} \int_{\lambda=-\epsilon}^{+\epsilon} J\,(\lambda,\ E,\ \xi)\ \frac{dA}{r^2}}{\int_{\phi} \int_{\lambda=-\epsilon}^{+\epsilon} \frac{dA \cos \xi}{r^2}} \tag{13}$$

The integral is over a strip of the earth's surface along the equator from the east limb to the west limb, and the distance r is measured from the area of integration to the point of observation. The denominator of this expression is the solid angle over which the directional flux is averaged, and the limit $\epsilon \to 0$ represents the fact that particles moving at right angles to the magnetic field vector on the equator must have emerged from the atmosphere at $\lambda = 0°$. Using equation (12), we get

$$J\,(R,\ 0°,\ E,\ 90°) \;=\; \frac{1}{\pi}\ J\,(0°,\ E)\ . \tag{14}$$

The number of decays from this neutron stream is given by

$$S\,(E) \;=\; \frac{\Lambda}{v\,(E)}\ J\,(R,\ 0°,\ E,\ 90°) \tag{15}$$

where $\Lambda = 9.9 \times 10^{-4}$ sec^{-1}

$v(E)$ = the velocity of a neutron of energy E

$S(E)$ = the decay rate in cm^{-3} sec^{-1} ster^{-1} MeV^{-1} .

Then the average source strength over a proton orbit is

$$\overline{S(E)} = \frac{g \Lambda}{\pi v(E)} J(0, E) \qquad (16)$$

where g is given by equation (9) and we have used equation (14). The integral of equation (16) from E=1 to ∞ gives the CRAND source strength to be compared with the value calculated from equation (8). An upper limit to this integral is given by

$$\int_1^\infty \overline{S(E)}\, dE < \frac{g \Lambda}{\pi v(1)} \int_1^\infty J(0, E)\, dE \ . \qquad (17)$$

Using Lingenfelter's values for J (0, E),

$$\int_1^\infty J(0, E)\, dE = .038 \text{ neutrons cm}^{-2} \text{ sec}^{-1} \ . \qquad (18)$$

Combining relations (9), (17), and (18), we can calculate an upper limit for the CRAND source strength at L = 2.1 and $\alpha = 90°$:

$$\int_1^\infty \overline{S(E)}\, dE < 1.4 \times 10^{-15} \text{ p cm}^{-3} \text{ sec}^{-1} \text{ ster}^{-1} .$$

This is a factor of 1000 short of the value of 2.0×10^{-12} cm^{-3} sec^{-1} ster^{-1} demanded by the measured flux.

3. SPAND

The detection of a large flux of low energy protons by Naugle and Kniffen [1962] led to the amplification of CRAND by the solar proton albedo neutron decay theory (SPAND). This theory supposes that the low energy trapped protons are the decay products of albedo neutrons generated in the polar atmosphere by low energy solar cosmic rays. Lenchek [1962] worked out the details of this model and concluded that SPAND could account for the measurements of Naugle and Kniffen. Since the observations of Davis and Williamson [1962], of Bame et al. [1963], and of Relay I [Fillius and McIlwain, 1964], however, it has been evident that SPAND was inadequate on at least three counts.

(1) The energy spectrum calculated for SPAND was Maxwellian with a temperature of about 4 MeV. This does not at all describe

the observed spectra, which vary throughout space but can be generalized as much softer than predicted, with enormous numbers of 100 keV particles.

(2) The geometry of SPAND forbids any trapping below L = 1.7 and allows no particles mirroring on the equator below L = 3.5. However, the largest fluxes observed by Relay I were on the equator, and many particles are observed below L = 1.7. The predicted and observed geometries are in violent disagreement.

(3) SPAND was only adequate to account for the intensity of 10 MeV protons observed by NERV at low altitudes. The intensity of 1 MeV Relay I protons at the equator on the same lines of force is 3 or 4 orders of magnitude greater. As pointed out in (1) and (2) above, the predicted energy and spatial variations are not such as to make up the difference. It must be concluded that SPAND is also too weak by several orders of magnitude.

The conclusion of this and the preceding section must be that, although cosmic ray and solar proton albedo mechanisms operate, they do not dominate. One must seek the controlling factors for inner zone protons elsewhere.

4. Diffusion Theories, 1

The observed numbers of low energy protons make it necessary to seek a source much stronger than neutron albedo. An obvious supply, of very generous magnitude, is the solar wind, and there has been revived interest in the early ideas of Kellogg [1959], Parker [1960], Herlofson [1960], and others. Injection is presumed to take place at the boundaries of the magnetosphere, and diffusion controls the particles' motion inward. Although a satisfactory diffusion equation has not been introduced and solved, one can look into several widely accepted constraints regarding the particles' behavior.

Following Parker, it has been popular to consider diffusion under which the first two adiabatic invariants are preserved and the third is broken [Davis and Chang, 1962; Nakada et al., 1964]. This has the effect of accelerating the particles to higher energies as they move inward towards the earth. The simplest case to observe experimentally is on the equator, where the second invariant is constant at zero. Figure 25 shows integral energy spectra at the equator which were constructed from Relay I data [Fillius and McIlwain, 1964]. With the first adiabatic invariant

held constant, the energy of a particle diffusing inward on the equator will vary as

$$E \alpha L^{-3} . \tag{19}$$

The phase space density, f, of particles is related to the measured flux by

$$JdE = f \; p^2 \; dE \tag{20}$$

where p is the particle momentum

j is the differential flux cm^{-2} sec^{-1} $ster^{-1}$ MeV^{-1} .

Figure 26 shows the differential flux on the equator obtained by differentiating the spectra in Figure 25. McIlwain [Private Communication, 1964] has used these values to construct a plot of f vs L for particles of constant μ on the equator (Figure 27). Several values of μ are represented, and the curves are labeled according to the energy of the particle at L = 2. Except for some small irregularities which were probably introduced in differentiating Figure 25, f is seen to decrease as the particles approach the earth. This is the same effect seen by Nakada et al., in analyzing Davis's data, and it has been widely

interpreted to mean that the source of these particles is outside the region of the measurements.

5. Diffusion Theories, 2

The particles on the equator do not tell the whole story, of course. Figures 28 and 29 give the complete distributions seen by Relay I, in R, λ, and B, L space, respectively. The six energy bands are arranged consecutively, so that one can scan from the low to the high energy particles, and the contour representing a flux of 10^3 has been darkened on Figure 31, so that one can compare the intensities. There is an unmistakable continuity in the development of the spatial distribution as energy range increases. These features are especially clear:

(1) The high energy particles are at lower L values.

(2) The intensity of the high energy particles is much less that the low energy particles.

(3) The distributions are related by a continuous development as one moves along the energy scale.

The first point above can be demonstrated effectively by looking at the equatorial profile of the radiation. If one plots the position of the peak of a profile against the energy

threshold of the detector, one obtains a very regular pattern. Figure 30 illustrates this using data from many different detectors on a host of satellites [Brown et al., 1963; Davis, 1965; Frank et al., 1964; Frank et al., 1965; Brown et al., 1964]. The relationship between threshold energy and position of the maximum is uniform over the three orders of magnitude measured. Further, if one extrapolates this relationship to find what energy would peak at the edge of the magnetosphere, one gets the proper value for the energy of protons in the solar wind. This is consistent with the idea that protons are injected into the magnetosphere with solar wind energies near the solar wind interface. Some diffuse inward, gaining energy, until they reach the atmosphere and are lost. Others diffuse outward and are lost again at the boundary. Figure 30 would then represent a schedule for this diffusion, a "main sequence" for the equatorial distribution.

The need for postulating outward diffusion and loss of particles has been seen in Figure 27, which shows that the particle density decreases as they go inward. It is also apparent in Figure 30. Knowing that the particles' second invariant is conserved, and assuming that the first invariant is also

constant, we expect the energy of any particle to vary according to equation (19):

$$E \propto L^{-3} \quad .$$

If there was no loss, the position of the peak intensity would follow this path (a 45° diagonal) across Figure 30. As it is, one sees that the particles which constitute the peak at 50 MeV lay inside the peak at 10 MeV and most of the particles from the 10 MeV peak must be lost. It may be noted that the number of particles off the peak at lower energies is sufficient to fill the peak at higher energies.

6. The Maximum Energy for Stable Trapping

It has been the concern of some theories to account for the non-trapping of high energy protons in the outer belt. (See the review papers by Haerendel [1964] and Singer and Lenchek [1962].) These theories are based on the breakdown of adiabatic motion in the decreasing magnetic field, and they all result in a maximum energy for stable trapping which decreases as one goes to higher altitudes. Efforts have been made to test these ideas by studying the change in the energy

spectrum throughout the region where breakdown should occur [McIlwain and Pizzella, 1963]. As the ratio of counting rates in two different energy ranges is a measure of the spectral slope, Relay I offers an excellent opportunity for such a study.

Figure 31 is a contour plot of a spectral ratio for low energy protons, and the interpretation of this ratio as a power law spectrum is given in Table IV. As a consequence of the nesting of the energy ranges, their ratio goes through a maximum as the spectrum goes monotonically from hard to soft. For an assumed power law spectrum the maximum ratio is 0.31; for an exponential, 0.41; and for a Maxwellian, 0.45. Between L = 1.5 and L = 2.1 the spectrum cannot be fitted by any of these curves, as the ratio is too high. This fact makes it difficult to present the data, and it can be interpreted to mean that the spectrum is highly curved in this region.

The figure shows that the spectrum is almost constant along each line of force and varies rapidly between lines. It is very soft at high L values and becomes harder at lower L in keeping with the adiabatic breakdown theories. If this model is adopted, Figure 30 can be used to evaluate the critical energy for stable trapping. The position of the maximum flux above a given energy is then

interpreted as the position where non-adiabatic losses begin to dominate over adiabatic losses, and the relationship between the critical L and E is

$$E = 450\ L^{-6.5} \quad . \tag{21}$$

The exponent of 6.5 in this relationship is higher than the exponent of 5.2 which McIlwain and Pizzella found for the L dependence of their spectral parameter E_o, and this in turn is higher than the value of 4 expected on theoretical grounds. As this discrepancy is sizable, the adiabatic breakdown theory is not supported on these grounds.

Comparing the Relay I high energy proton spectrum with adiabatic breakdown theory produces an immediate contradiction. The ratio of two high energy channels is plotted in Figure 32, and Table IV again gives the power law interpretation. The spectrum is constant from L = 2.0 to 2.5. It is softest at L = 1.9 on the equator and becomes much harder at lower L. From L = 1.9 to 2.5 the spectrum actually becomes harder. This trend violates the most fundamental result of the adiabatic breakdown theories, that the maximum trapping energy should

decrease at higher altitudes. On the basis of this data one is forced to conclude that some other process controls the energy spectrum of inner zone protons.

V. SUMMARY

From December 1962 to September 1963 the inner zone proton belt remained steady enough to permit a thorough mapping of the energy spectrum and spatial distribution by the SUI-UCSD equipment aboard Relay I. Eight energy ranges from 1.1 to 63 MeV reach their maximum intensities at the equator, and the variation away from the equator on a line of force can be expressed as the third or fourth power of 1/B. The distribution of high energy protons lies closer to the earth than that of low energy protons, and the radial distance to the peak intensity above an energy threshold E varies as $E^{-.154}$. Low energy protons exhibit the highest intensities, illustrative values being $j_{\perp} = 3.7 \times 10^{6}$ protons cm^{-2} sec^{-1} $ster^{-1}$ from 1.1 to 14 MeV at L = 2.2 at the equator, and $j_{\perp} = 1.6 \times 10^{4}$ protons cm^{-2} sec^{-1} $ster^{-1}$ from 18.2 to 25 MeV at L = 1.6 on the equator.

The Relay I measurements have been compared with seven other experiments in the same region of space from 1960 through 1964 and there is typically agreement within 50%. As time intensities greater than this have been observed by both Relay I and Explorer VII, it is not safe to assume that there have been

no changes in this period, and it may be that the intensities return to the same levels after each change. In correlating the results of many other experiments, Relay I shows the value of a comprehensive treatment of the inner zone.

Neutron albedo sources, both cosmic ray and solar proton produced sources, are too weak to produce the intensities of low energy protons. A calculation with CRAND shows a shortcoming by a factor of over 1000, and SPAND appears too weak by the same factor. Additionally, the energy spectrum and spatial distribution eliminates SPAND as a major source.

Injection and diffusion of solar wind protons is considered as a possible source, and it is seen that the density of particles decreases as one approaches the earth, as expected. The mechanism of the diffusion is unknown, and the constraints placed on the diffusing particles may not be as simple as supposed. Specifically, diffusion constrained by preservation of the first two adiabatic invariants can be reconciled with the observations only by invoking an energy dependent loss process. More theoretical work is needed to clarify the expected results.

Adiabatic breakdown theories place an upper limit on the energy of protons which are trappable in the magnetic field, and the data have been examined to evaluate this as a controlling mechanism. The spectrum of low energy protons shows the qualitatively expected trend, becoming harder at lower L values. However, the cutoff energy evaluated on this model shows the wrong L-dependence, varying as $L^{-6.5}$ rather than the predicted L^{-4}. Furthermore, the energy spectrum of high energy protons contradicts this model conclusively, the spectrum actually becoming harder at higher L values. Other mechanisms must be found to account for the spatial variations of the trapped proton spectrum.

TABLE I

Summary of Detector Characteristics

Detector B

Sensor:	Silicon surface-barrier diode with depletion depth of 25 mg/cm^2.
Geometric factor:	.0136 cm^2-ster (directional).
Shielding:	8.5 gm/cm^2 brass in sides and back. 1.115 mg/cm^2 (air equivalent) nickel light shield over look cone.

Electronic discrimination levels:

B_α	=	0.87 MeV
B_β	=	1.41 MeV
B_γ	=	2.11 MeV
B_δ	=	3.84 MeV

Proton energy ranges:

Range one:	1.1 to 1.6 MeV and
	7.1 to 14 MeV
Range two:	1.6 to 2.25 MeV and
	4.75 to 7.1 MeV
Range three:	2.25 to 4.7 MeV

TABLE I
(continued)

Detector C

Sensors: Two silicon Li-drift diodes with active depths of 107 and 132 mg/cm^2, operated in coincidence.

Geometric factor: 0.22 cm^2 ster (directional).

Electronic discrimination levels:

Cl_α	=	0.75	MeV
Cl_β	=	1.71	MeV
Cl_γ	=	2.84	MeV
$C2_\alpha$	=	1.14	MeV
$C2_\beta$	=	2.04	MeV
$C2_\gamma$	=	3.53	MeV

Proton energy ranges:

Range one:	18.2	to 25	MeV
Range two:	25	to 35	MeV
Range three:	35	to 63	MeV

Directionality

These detectors are mounted perpendicular to the satellite spin axis and are gated by a magnetometer to record data only when they point within $\pm$ 10 degrees of the plane perpendicular to the local magnetic field vector. Thus they measure $j_\perp$, the flux of locally mirroring particles.

TABLE II

Nominal Orbital Parameters of Relay I

Inclination	47.5 degrees
Anomalistic Period	185 minutes
Height of Perigee	1.2 earth radii
Height of Apogee	2.2 earth radii
Spin Rate	27 revolutions/sec
Date of Launch	December 13, 1962

TABLE III

Supplementary Detector Characteristics

	Detector A
Sensor:	0.9 cm sphere of plastic scintillator
Geometric factor:	0.33 cm^2 omnidirectional
Shielding:	1.3 gm/cm^2 Al over one hemisphere
Proton Range:	> 33.5 MeV

	Detector D
Sensor:	0.25 cm cylinder of plastic scintillator
Geometric factor:	.0027 cm^2-ster directional
Proton Range:	> 5.2 MeV

TABLE IV

n *	$\frac{N(2.25 \leq E \leq 4.7)}{N(1.1 \leq E \leq 14)}$	$\frac{N(35 \leq E \leq 63)}{N(25 \leq E \leq 63)}$
.2	.302	.61
.4	.304	.59
.6	.305	.57
.8	.292	.55
1.0	.279	.53
1.2	.263	.50
1.4	.245	.48
1.6	.226	.46
1.8	.206	.44
2.0	.187	.42
2.2	.168	.40
2.4	.150	.38
2.6	.133	.36
2.8	.118	.34
3.0	.105	.32
3.4	.081	.29
3.8	.062	.26
4.2	.047	.23
4.6	.036	.20
5.0	.027	.18

*for a spectrum of the form $N(>E) = N_o E^{-n}$.

BIBLIOGRAPHY

Armstrong, A. H., F. B. Harrison, H. H. Heckman, and L. Rosen, Charged particles in the inner Van Allen belt, J. Geophys. Res., 66, 351-357, 1961.

Bame, S. J., J. P. Conner, H. H. Hill, and F. E. Holly, Protons in the outer zone of the radiation belt, J. Geophys. Res., 68, 55-63, 1963.

Bostrom, C. O., A. J. Zmuda, and G. F. Pieper, Trapped protons in the South Atlantic magnetic anomaly, July through December 1961. 2. Comparisons with Nerv and Relay I and discussion of the energy spectrum, J. Geophys. Res., 70, 2035-2044, 1965.

Brown, W. L., L. W. Davidson, and L. V. Medford, The energetic particle environment of Relay I: Bell Telephone Laboratory experiment, Bell Telephone Laboratory, Summit, New Jersey, 1964.

Brown, W. L., J. D. Gabbe, and W. Rosenzweig, Results of the Telstar radiation experiments, The Bell System Technical Journal, 42, No. 4, Part 2, 1505-1559, July, 1963.

Davis, Leverett, and D. B. Chang, On the effect of geomagnetic fluctuations on trapped particles, J. Geophys. Res., 67, 2169-2179, 1962.

Davis, L. R., Low energy trapped protons and electrons, Proc. of the Plasma Space Science Symposium, D. Reidel Pub. Co., Dordrecht, Holland, 1965 a.

Davis, L. R., Private Communication, 1965 b

Davis, L. R., and J. M. Williamson, Low-energy trapped protons, Space Research III, Proceedings of the Third International Space Science Symposium, North-Holland Publishing Company, Amsterdam, 1963, pp. 365-375.

Dearnally, G., Semiconductor counters for nuclear radiation, Chapter 10, John Wiley, Inc., New York, 1963.

Fillius, R. W., Satellite instruments using solid state detectors, Research Report SUI 63-26, Department of Physics and Astronomy, The State University of Iowa, Iowa City, Iowa, 1963.

Fillius, R. W., and C. E. McIlwain, Solid state detectors for inner zone protons, Space Research III, Proceedings of the Third COSPAR Symposium, Washington, D. C., April-May, 1962, pp. 1122-1128, North-Holland Publishing Co., Amsterdam.

Fillius, R. W., and C. E. McIlwain, Anomalous energy spectrum of protons in the earth's radiation belt, Phys. Rev. Letters, 12, 609-612, 1964.

Fillius, R. W., and C. E. McIlwain, A survey of inner space protons, Department of Physics, University of California San Diego, April, 1965.

Frank, L. A., J. A. Van Allen, and H. K. Hills, A study of charged particles in the earth's outer radiation zone with Explorer 14, J. Geophys. Res., 69, 2171-2191, 1964.

Frank, L. A., J. A. Van Allen, H. K. Hills, and R. W. Fillius, Proton and electron intensities in the earth's outer radiation zone: OGO 1, Abstract, Trans. Am. Geophys. Union, 46, p. 124, March, 1965.

Freden, S. C., J. B. Blake, and G. A. Paulikas, Spatial variations of the inner zone trapped proton spectrum, Aerospace Corporation, El Segundo, California, 1965.

Freden, S. C., and George A. Paulikas, Trapped protons at low altitudes in the South Atlantic magnetic anomaly, J. Geophys. Res., 69, 1259-1269, 1964.

Freden, S. C., and R. Stephen White, Protons in the earth's magnetic field, Phys. Rev. Letters, 3, 9-10, 1959.

Haerendel, G., Protonen im Inneren Strahlungsgurtel, Fortschritte der Physik, 12, 271-346, 1964.

Hassitt, A., An average atmosphere for particles trapped in the earth's magnetic field, Research Report, Department of Physics, University of California San Diego, La Jolla, California.

Herlofson, N., Diffusion of particles in the earth's radiation belts, Phys. Rev. Letters, 5, 414-416, 1960.

Hess, W. N., E. H. Canfield, and R. E. Lingenfelter, Cosmic-ray neutron demography, J. Geophys. Res., 66, 665-678, 1961.

Imhof, W. L., and R. V. Smith, Proton intensities and energy spectrums in the inner Van Allen belt, J. Geophys. Res., 69, 91-100, 1964.

Kellogg, P. J., Van Allen radiation of solar origin, Nature, 183, 1295, 1959.

Krimigis, S. M., and J. A. Van Allen, Observations of geomagnetically trapped protons with Injun 4, Trans. AGU, 46, March, 1965, Abstract, p. 140.

Lenchek, A. M., On the anomalous component of low-energy geomagnetically trapped protons, J. Geophys. Res., 67, 2145-2168, 1962.

Lingenfelter, R. E., The cosmic-ray neutron leakage flux, J. Geophys. Res., 68, 5633-5639, 1963.

McIlwain, C. E., Coordinates for mapping the distribution of magnetically trapped particles, J. Geophys. Res., 66, 3681-3691, 1961.

McIlwain, C. E., The radiation belts, natural and artificial, Science, 142, 355-361, October 18, 1963.

McIlwain, C. E., Redistribution of trapped protons during a magnetic storm, paper delivered at 1964 COSPAR symposium, Milan, Italy.

McIlwain, C. E., Private Communication, 1965.

McIlwain, C. E., R. W. Fillius, J. Valerio, and A. Dave, Relay I trapped radiation measurements, NASA TN D-2516, December, 1964.

Nakada, M. P., J. W. Dungey, and W. N. Hess, Theoretical studies of protons in the outer radiation belt, Report X-640-44-110, NASA/GSFC, Greenbelt, Md.

Naugle, John E., and D. A. Kniffen, The flux and energy spectra of the protons in the inner Van Allen belt, J. Phys. Soc. Japan, 17, Supplement A-11, 1962, International Conference on Cosmic Rays and the Earth Storm, Part II, 118-122.

Naugle, J. E., and D. A. Kniffen, Variations of the proton energy spectrum with positron in the inner Van Allen belt, J. Geophys. Res., 68, 4065-4078, 1963.

Parker, E. N., Geomagnetic fluctuations and the form of the outer zone of the Van Allen radiation belt, J. Geophys. Res., 65, 3117-3130, 1960.

Peterson, L. E., Radioactivity induced in Na I by trapped protons, J. Geophys. Res., 70, 1762-1765, 1965.

Pizzella, G., C. E. McIlwain, and J. A. Van Allen, Time variations of intensity in the earth's inner radiation zone, October 1959 through December 1960, J. Geophys. Res., 67, 1235-1253, 1962.

Ray, E. C., On the theory of protons trapped in the earth's magnetic field, J. Geophys. Res., 65, 1125-1134, 1960.

Singer, S. F., Trapped albedo theory of the radiation belt, Phys. Rev. Letters, 1, 181, 1959.

Singer, S. F., and A. M. Lenchek, Geomagnetically trapped radiation, Progress in Elementary Particle and Cosmic Ray Physics, Vol. VI, North-Holland Publishing Co., Amsterdam, 1962.

Valerio, J., Protons from 40 to 110 MeV observed on Injun 3, J. Geophys. Res., 69, 4949-4958, 1964.

Van Allen, J. A., The geomagnetically-trapped corpuscular radiation, J. Geophys. Res., 64, 1683-1689, 1959.

Vernov, S. N., and A. E. Chudakov, Terrestrial corpuscular radiation and cosmic rays, Space Research, Proceedings of the First International Space Science Symposium, Nice, 1960, pp. 751-796, North-Holland Publishing Company, Amsterdam, 1960.

APPENDIX

Method for Computing a Gain-Shift Correction

Many samples of data have shown that the best fit to the pulse height spectrum is an exponential:

$$N (> H_i) = N \exp (- s H_i) \qquad \text{(A-1)}$$

where H_i is one of the discrimination levels

$N (> H_i)$ is the number of pulses above H_i

s is computed from the data.

If the discrimination level is H_i and we want to know the number of pulses above some nearby level H_{io}, this is given by

$$N (> H_{io}) = [\exp (s (H_i - H_{io}))] N (> H_i) . \qquad \text{(A-2)}$$

In using this formula we compute s from two nearby levels H_j and H_k,

$$s = \frac{\ln (N (> H_j) / N (> H_k)}{H_k - H_j} \qquad \text{(A-3)}$$

These formulas are used to compute a correction to the data when the detector gain has shifted because of temperature or radiation damage. Then,

H_{io} is the calibrated discrimination level

H_i is the shifted level

H_j and H_k are the two nearest levels.

FIGURE CAPTIONS

Figure 1. Corrections to detector B data.

Figure 2. The intensity on several lines of force, 1.1 to 14 MeV protons.

Figure 3. The intensity on several lines of force, 1.6 to 7.1 MeV protons.

Figure 4. The intensity on several lines of force, 2.25 to 4.7 MeV protons.

Figure 5. The intensity on several lines of force, 18.2 to 25 MeV protons.

Figure 6. The intensity on several lines of force, 25 to 35 MeV protons.

Figure 7. The intensity on several lines of force, 35 to 63 MeV protons.

Figure 8. The intensity on several lines of force, 18.2 to 63 MeV protons.

Figure 9. Contour map in B, L space, 1.1 to 14 MeV protons.

Figure 10. Contour map in B, L space, 1.6 to 7.1 MeV protons.

Figure 11. Contour map in B, L space, 2.25 to 4.7 MeV protons.

Figure 12. Contour map in B, L space, 18.2 to 25 MeV protons.

Figure 13. Contour map in B, L space, 25 to 35 MeV protons.

Figure 14. Contour map in B, L space, 35 to 63 MeV protons.

Figure 31. Contour map of spectral ratio at low energies.

Figure 32. Contour map of spectral ratio at high energies.

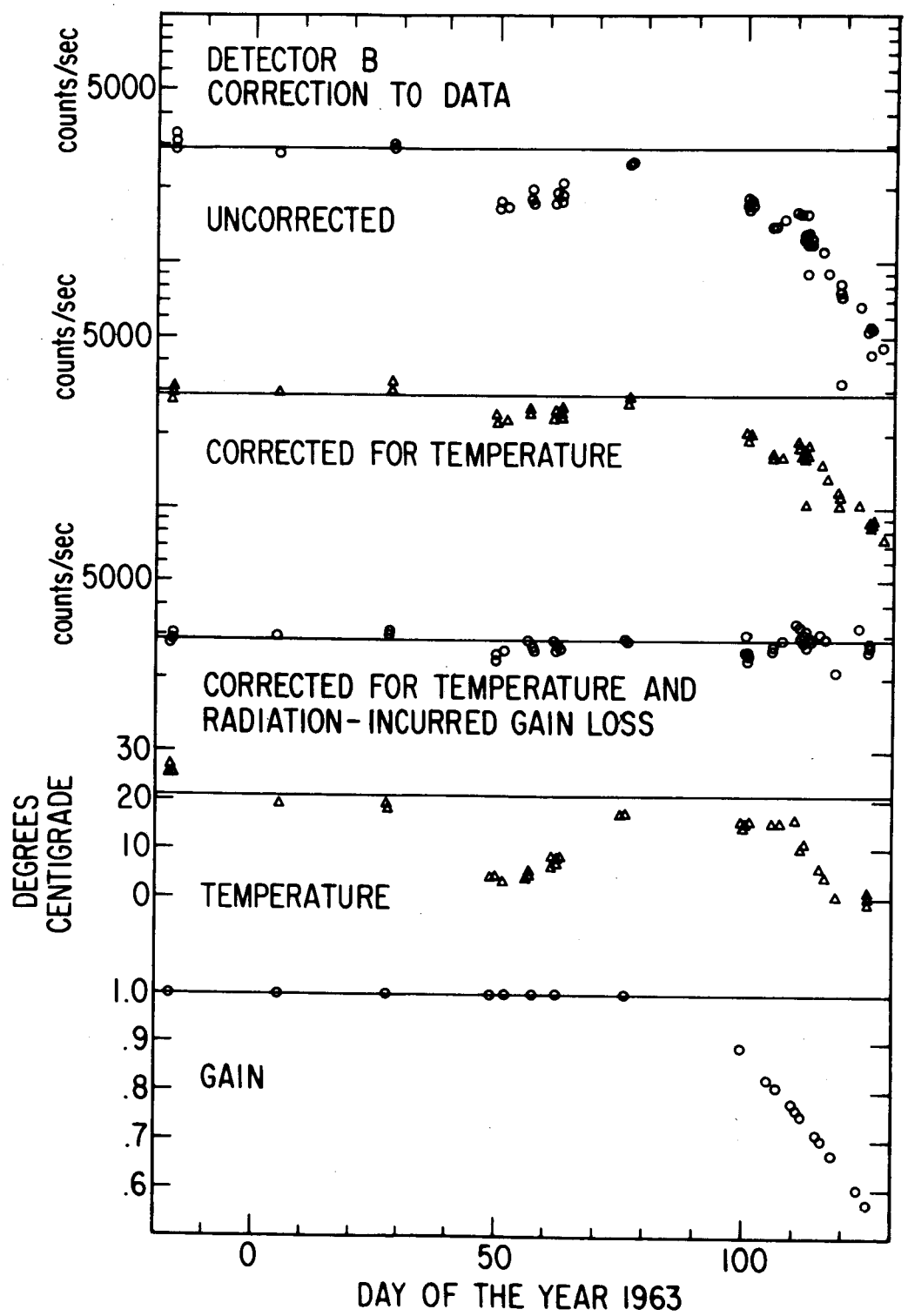
DETECTOR B
CORRECTION TO DATA
UNCORRECTED
CORRECTED FOR TEMPERATURE
CORRECTED FOR TEMPERATURE AND
RADIATION-INCURRED GAIN LOSS
TEMPERATURE
GAIN
counts/sec
5000
counts/sec
5000
counts/sec
5000
DEGREES
CENTIGRADE
30
20
10
0
1.0
.9
.8
.7
.6
0
50
100
DAY OF THE YEAR 1963

Figure 1

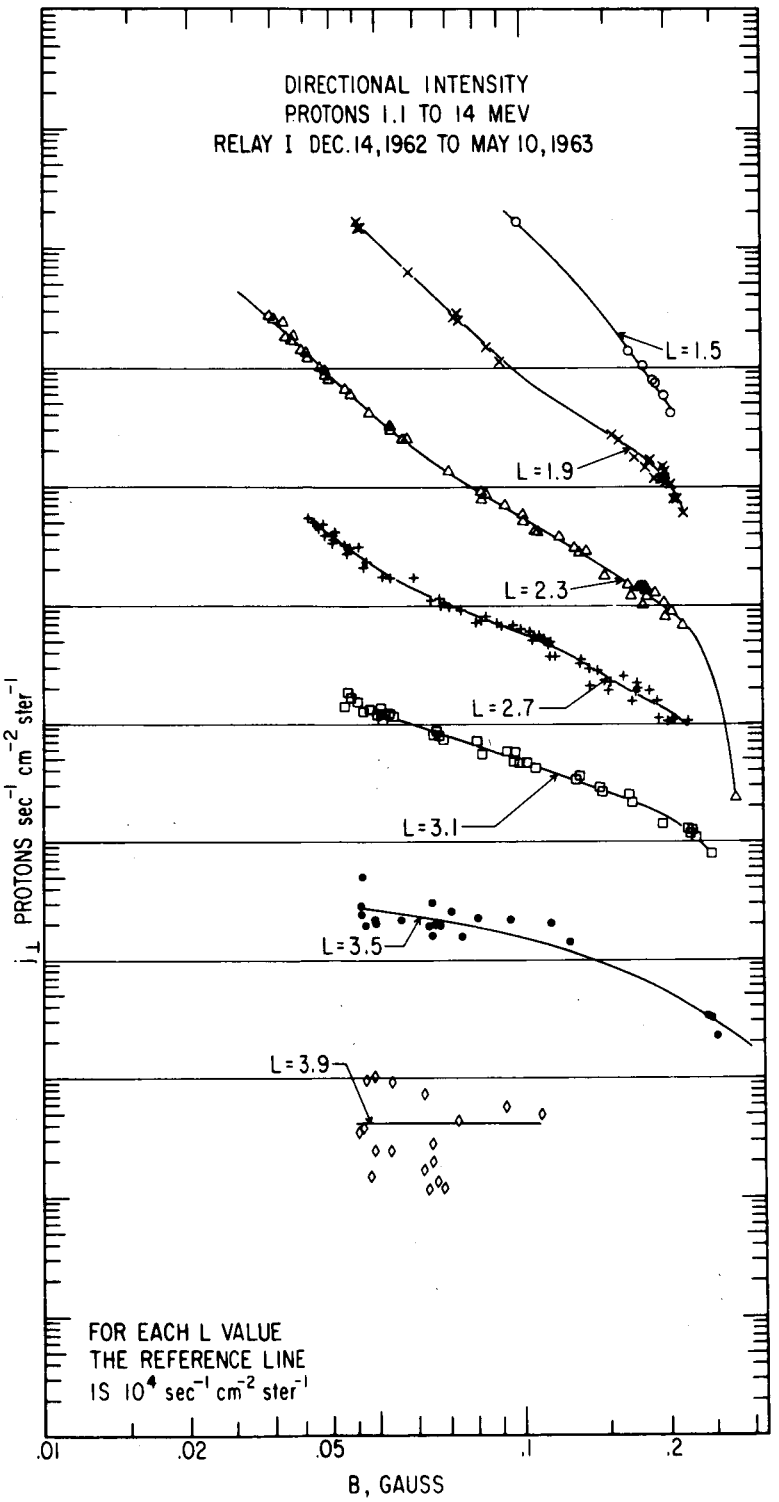
DIRECTIONAL INTENSITY
PROTONS 1.1 TO 14 MEV
RELAY I DEC. 14, 1962 TO MAY 10, 1963
L=1.5
L=1.9
L=2.3
L=2.7
L=3.1
L=3.5
L=3.9
FOR EACH L VALUE
THE REFERENCE LINE
IS 10^4 sec^{-1} cm^{-2} ster^{-1}
$j_\perp$ PROTONS sec^{-1} cm^{-2} ster^{-1}
.01
.02
.05
.1
.2
B, GAUSS

Figure 2

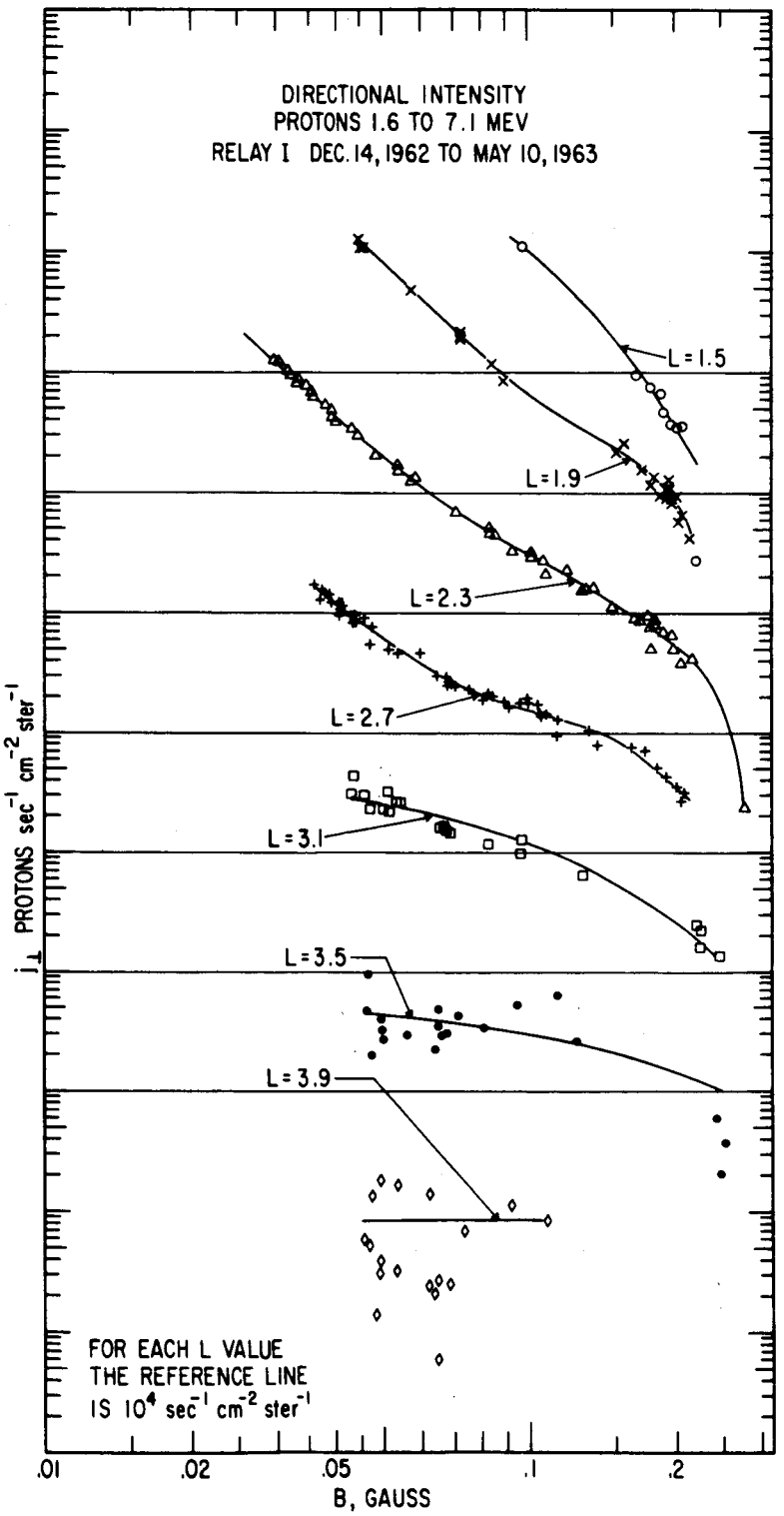
DIRECTIONAL INTENSITY
PROTONS 1.6 TO 7.1 MEV
RELAY I DEC. 14, 1962 TO MAY 10, 1963
L=1.5
L=1.9
L=2.3
L=2.7
L=3.1
L=3.5
L=3.9
FOR EACH L VALUE
THE REFERENCE LINE
IS 10⁴ sec⁻¹ cm⁻² ster⁻¹
j⊥ PROTONS sec⁻¹ cm⁻² ster⁻¹
.01
.02
.05
.1
.2
B, GAUSS

Figure 3

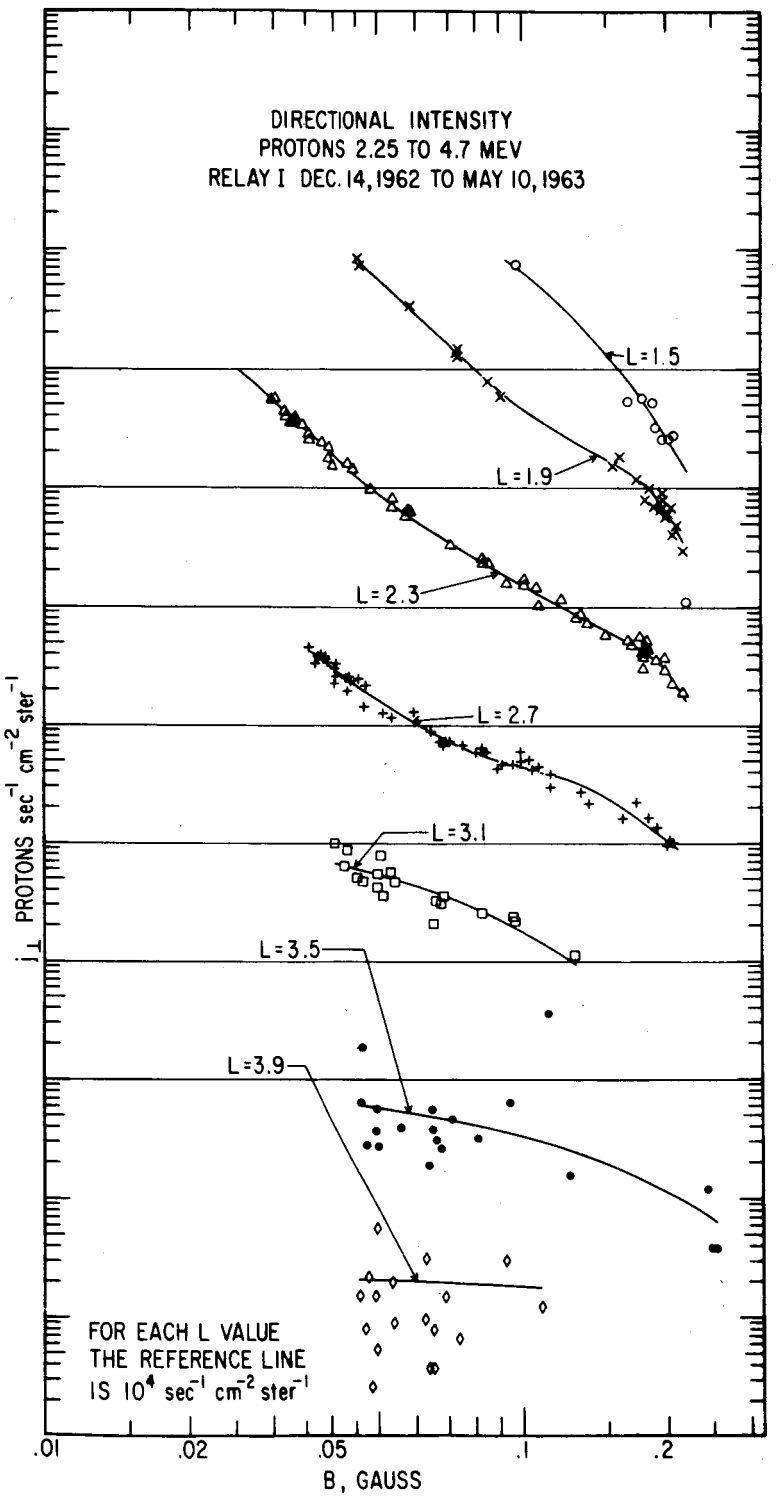
DIRECTIONAL INTENSITY
PROTONS 2.25 TO 4.7 MEV
RELAY I DEC. 14, 1962 TO MAY 10, 1963
L=1.5
L=1.9
L=2.3
L=2.7
L=3.1
L=3.5
L=3.9
FOR EACH L VALUE
THE REFERENCE LINE
IS 10^4 sec^{-1} cm^{-2} ster^{-1}
$j_\perp$ PROTONS sec^{-1} cm^{-2} ster^{-1}
.01
.02
.05
.1
.2
B, GAUSS

Figure 4

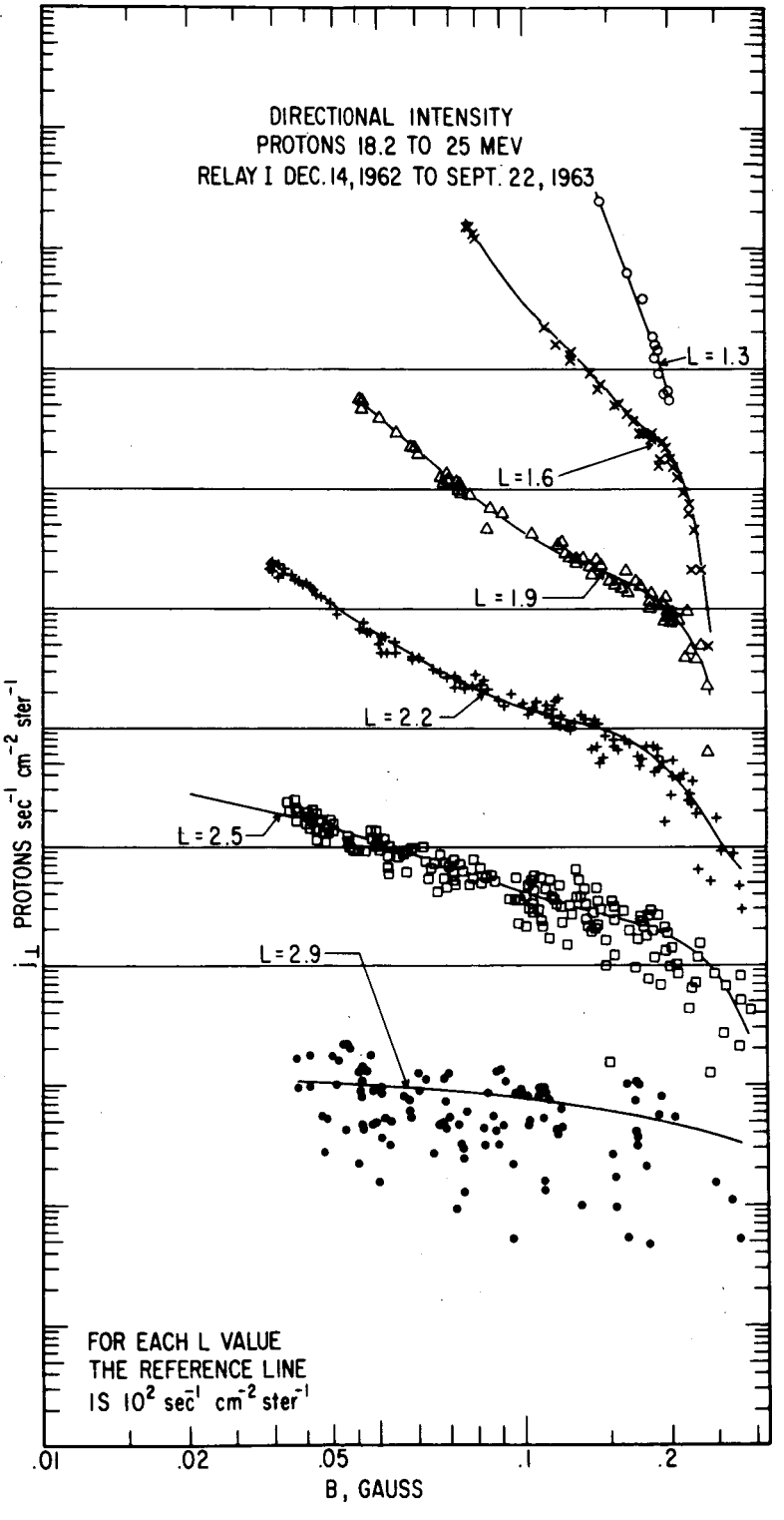
DIRECTIONAL INTENSITY
PROTONS 18.2 TO 25 MEV
RELAY I DEC. 14, 1962 TO SEPT. 22, 1963
L = 1.3
L = 1.6
L = 1.9
L = 2.2
L = 2.5
L = 2.9
j⊥ PROTONS sec⁻¹ cm⁻² ster⁻¹
FOR EACH L VALUE
THE REFERENCE LINE
IS 10² sec⁻¹ cm⁻² ster⁻¹
.01
.02
.05
.1
.2
B, GAUSS

Figure 5

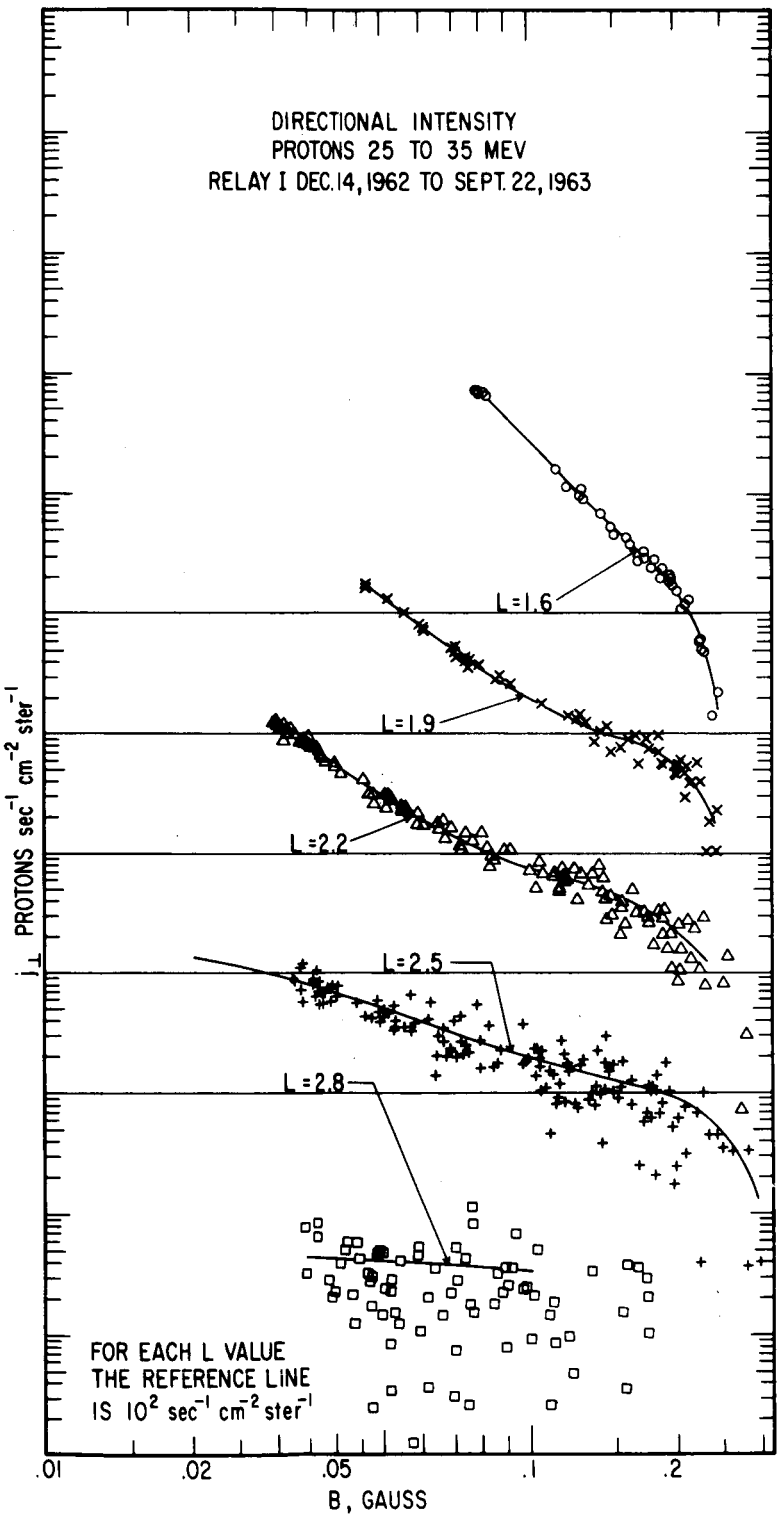
DIRECTIONAL INTENSITY
PROTONS 25 TO 35 MEV
RELAY I DEC.14, 1962 TO SEPT. 22, 1963
L=1.6
L=1.9
L=2.2
L=2.5
L=2.8
FOR EACH L VALUE
THE REFERENCE LINE
IS 10^2 sec^{-1} cm^{-2} ster^{-1}
$j_\perp$ PROTONS sec^{-1} cm^{-2} ster^{-1}
.01
.02
.05
.1
.2
B, GAUSS

Figure 6

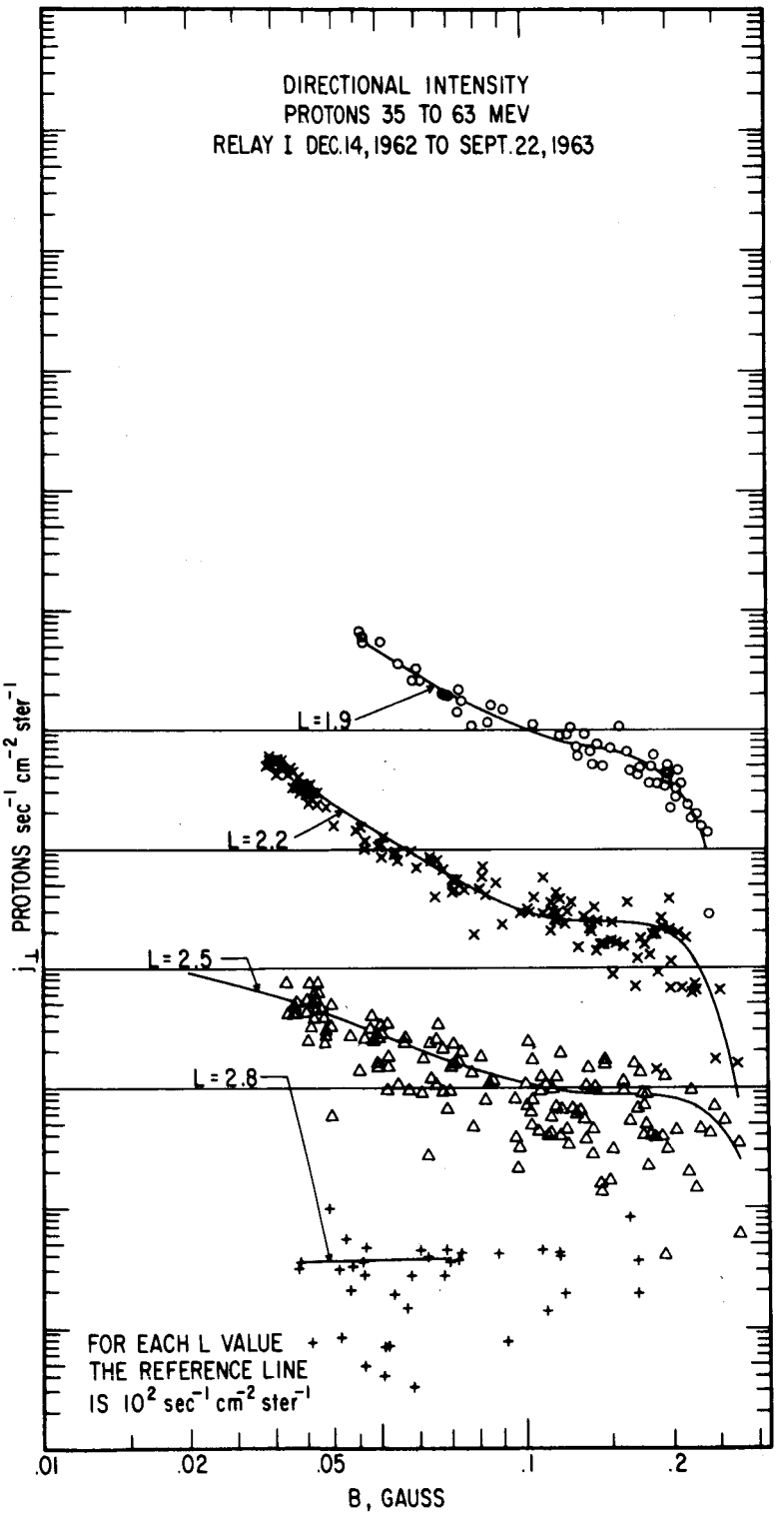
DIRECTIONAL INTENSITY
PROTONS 35 TO 63 MEV
RELAY I DEC.14, 1962 TO SEPT.22, 1963
L=1.9
L=2.2
L=2.5
L=2.8
FOR EACH L VALUE
THE REFERENCE LINE
IS 10^2 sec^{-1} cm^{-2} ster^{-1}
$j_\perp$ PROTONS sec^{-1} cm^{-2} ster^{-1}
.01
.02
.05
.1
.2
B, GAUSS

Figure 7

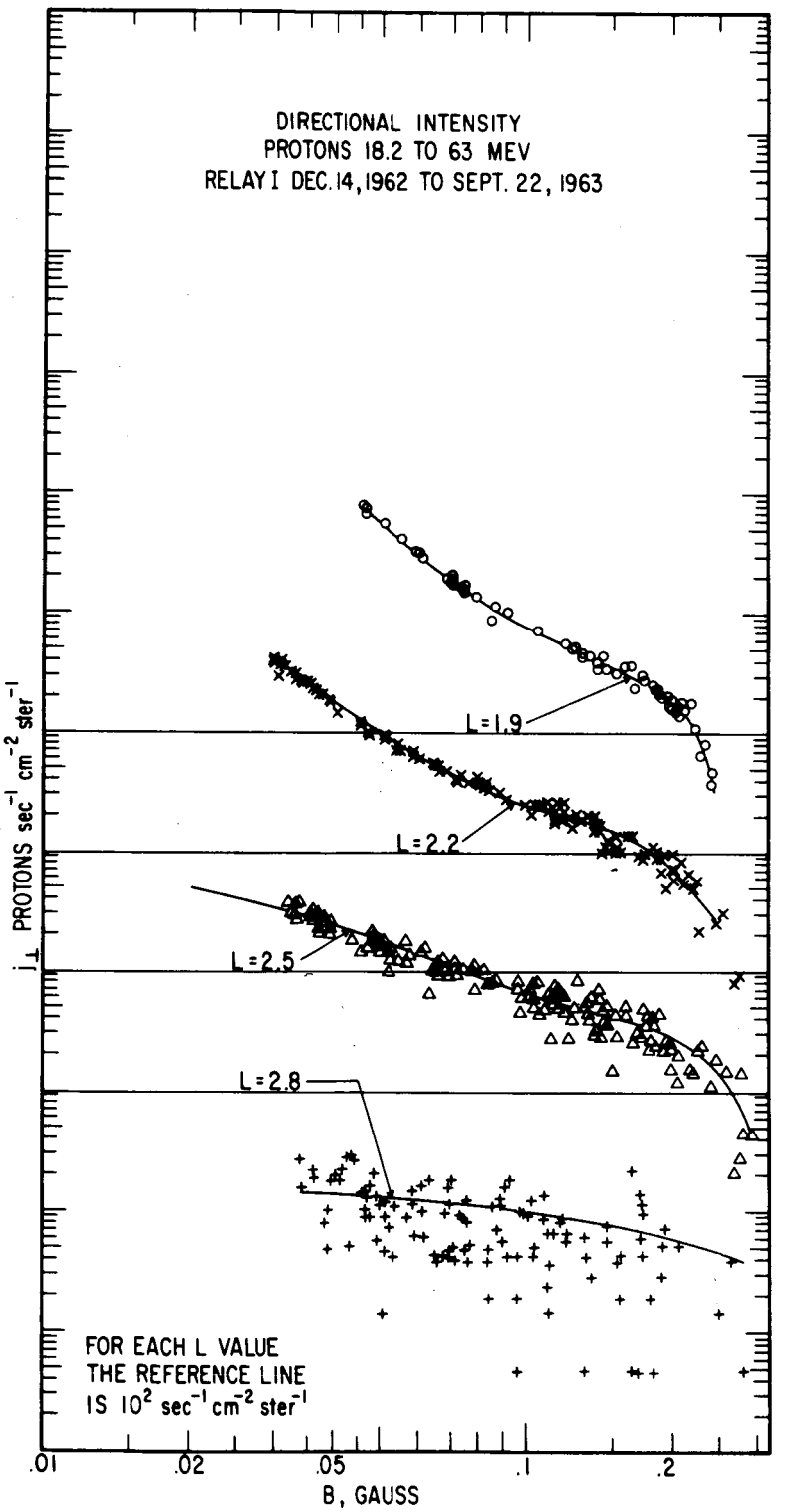
DIRECTIONAL INTENSITY
PROTONS 18.2 TO 63 MEV
RELAY I DEC. 14, 1962 TO SEPT. 22, 1963
L=1.9
L=2.2
L=2.5
L=2.8
FOR EACH L VALUE
THE REFERENCE LINE
IS 10^2 sec^{-1} cm^{-2} ster^{-1}
$j_\perp$ PROTONS sec^{-1} cm^{-2} ster^{-1}
.01
.02
.05
.1
.2
B, GAUSS

Figure 8

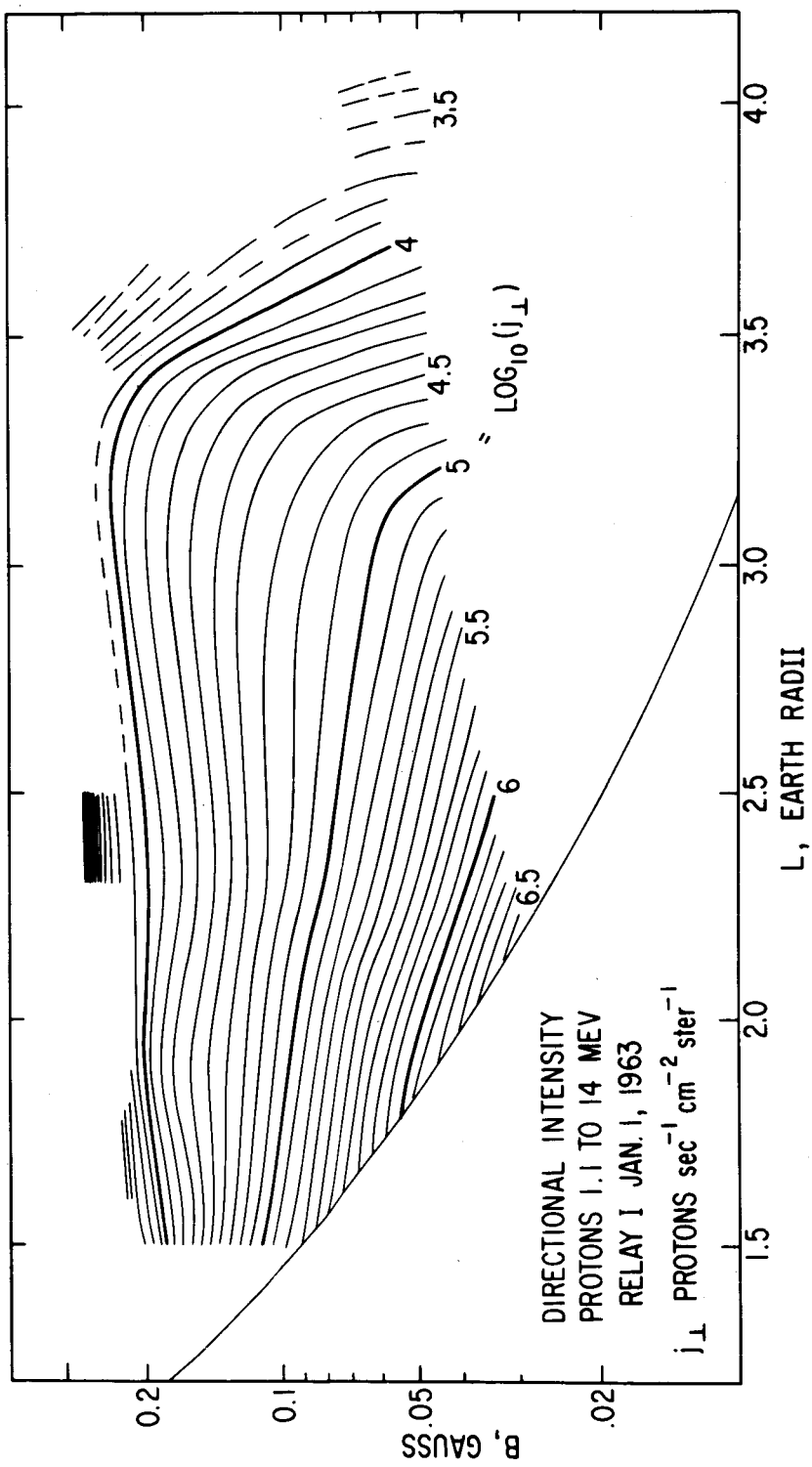
DIRECTIONAL INTENSITY
PROTONS 1.1 TO 14 MEV
RELAY I JAN. 1, 1963
$j_\perp$ PROTONS $sec^{-1} cm^{-2} ster^{-1}$
$= LOG_{10}(j_\perp)$
3.5
4
4.5
5
5.5
6
6.5
B, GAUSS
0.2
0.1
.05
.02
1.5
2.0
2.5
3.0
3.5
4.0
L, EARTH RADII

Figure 9

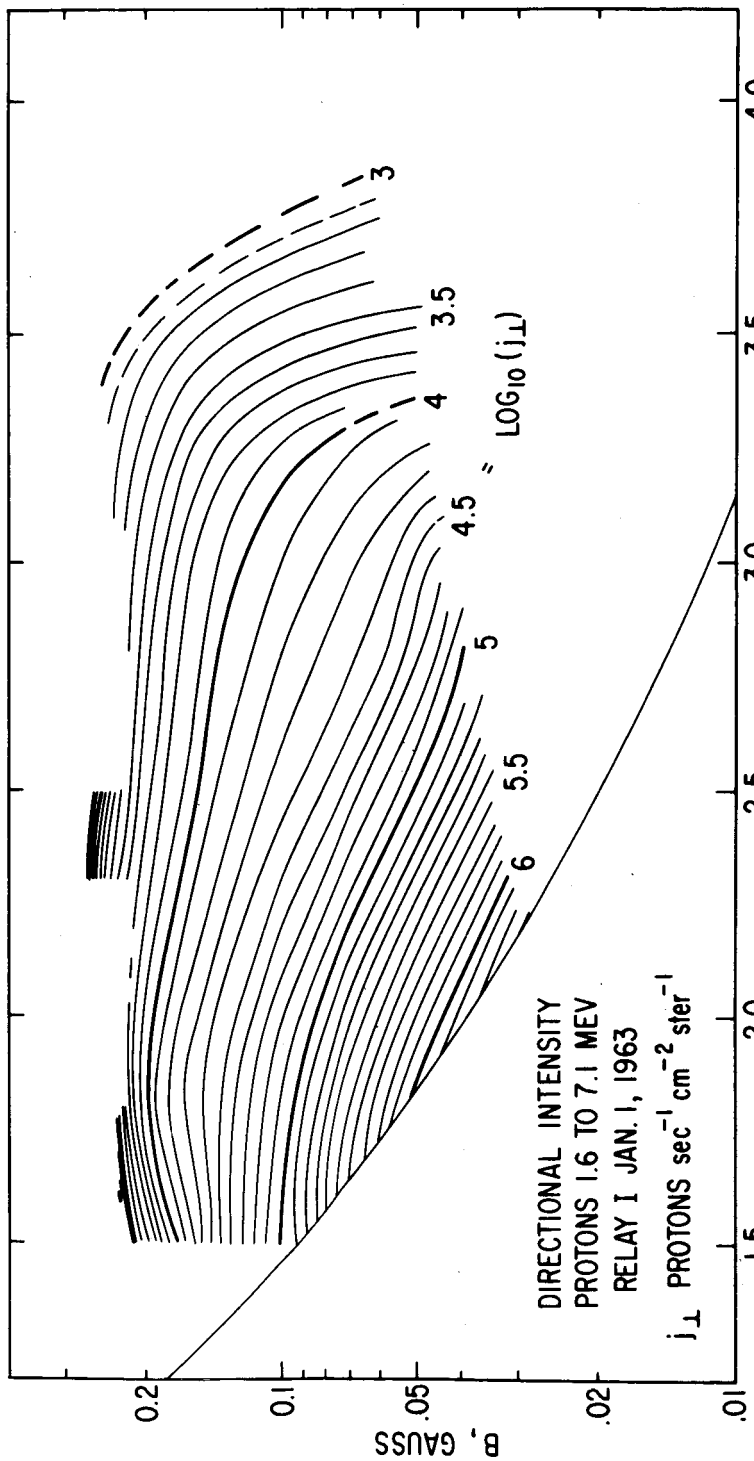
DIRECTIONAL INTENSITY
PROTONS 1.6 TO 7.1 MEV
RELAY I JAN. 1, 1963
$j_\perp$ PROTONS $sec^{-1} cm^{-2} ster^{-1}$
$LOG_{10}(j_\perp)$ =
3
3.5
4
4.5
5
5.5
6
B, GAUSS
0.2
0.1
.05
.02
.01
L, EARTH RADII
1.5
2.0
2.5
3.0
3.5
4.0

Figure 10

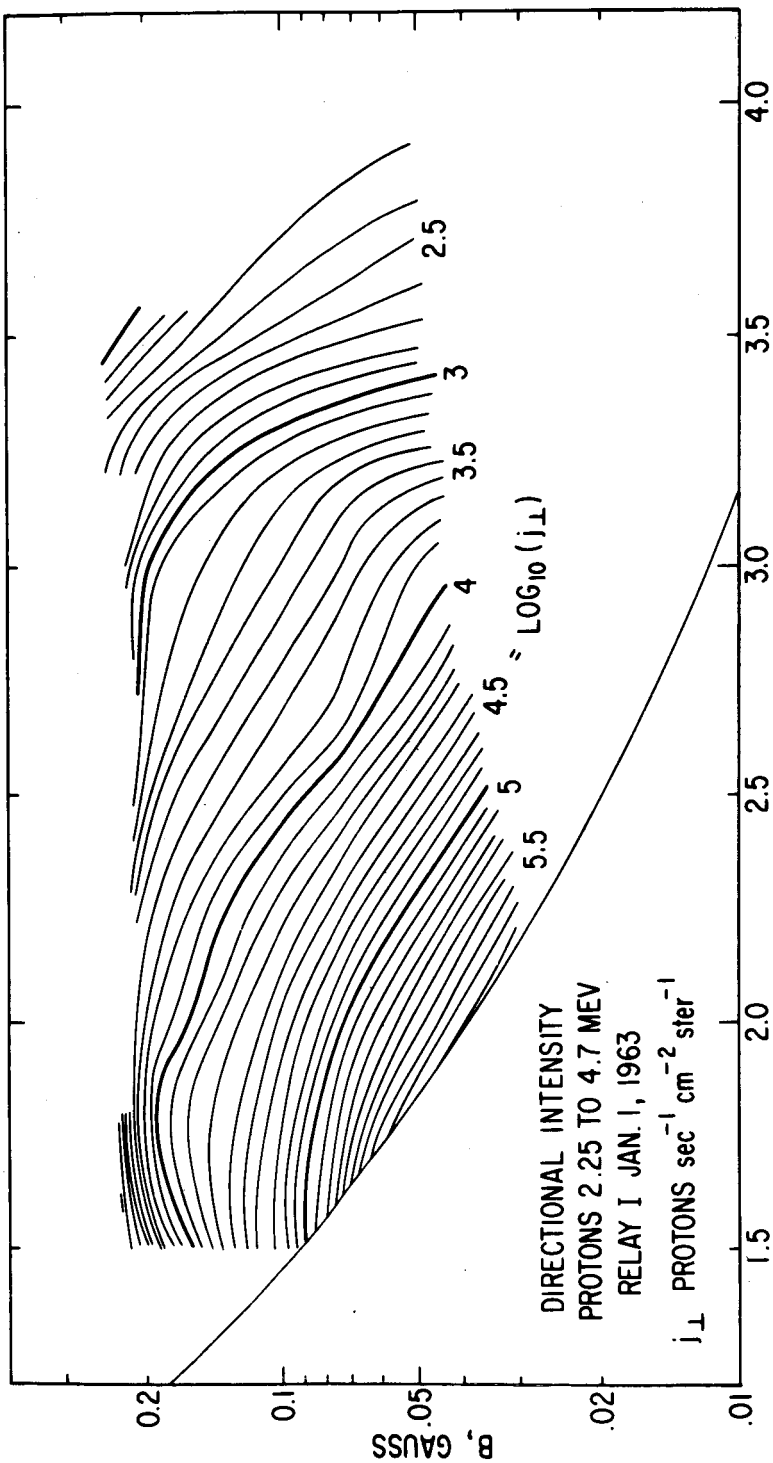
DIRECTIONAL INTENSITY
PROTONS 2.25 TO 4.7 MEV
RELAY I JAN. 1, 1963
$j_\perp$ PROTONS $sec^{-1}\ cm^{-2}\ ster^{-1}$
$= LOG_{10}(j_\perp)$
5.5
5
4.5
4
3.5
3
2.5
B, GAUSS
0.2
0.1
.05
.02
.01
1.5
2.0
2.5
3.0
3.5
4.0
L, EARTH RADII

Figure 11

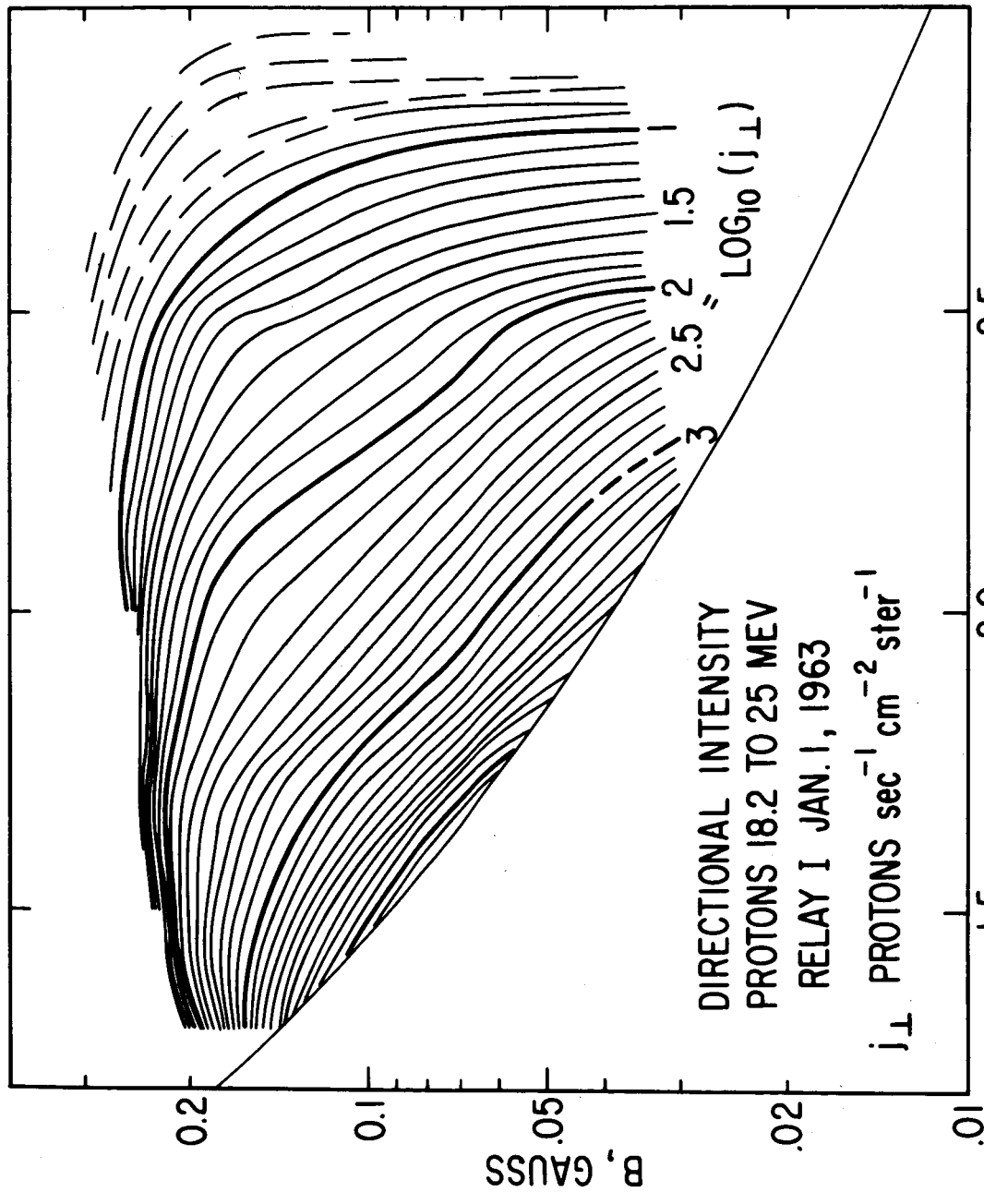
B, GAUSS
0.2
0.1
.05
.02
.01
1.5
2.0
2.5
L, EARTH RADII
DIRECTIONAL INTENSITY
PROTONS 18.2 TO 25 MEV
RELAY I JAN. 1, 1963
$j_\perp$ PROTONS $sec^{-1} cm^{-2} ster^{-1}$
$= LOG_{10}(j_\perp)$
1
1.5
2
2.5
3

Figure 12

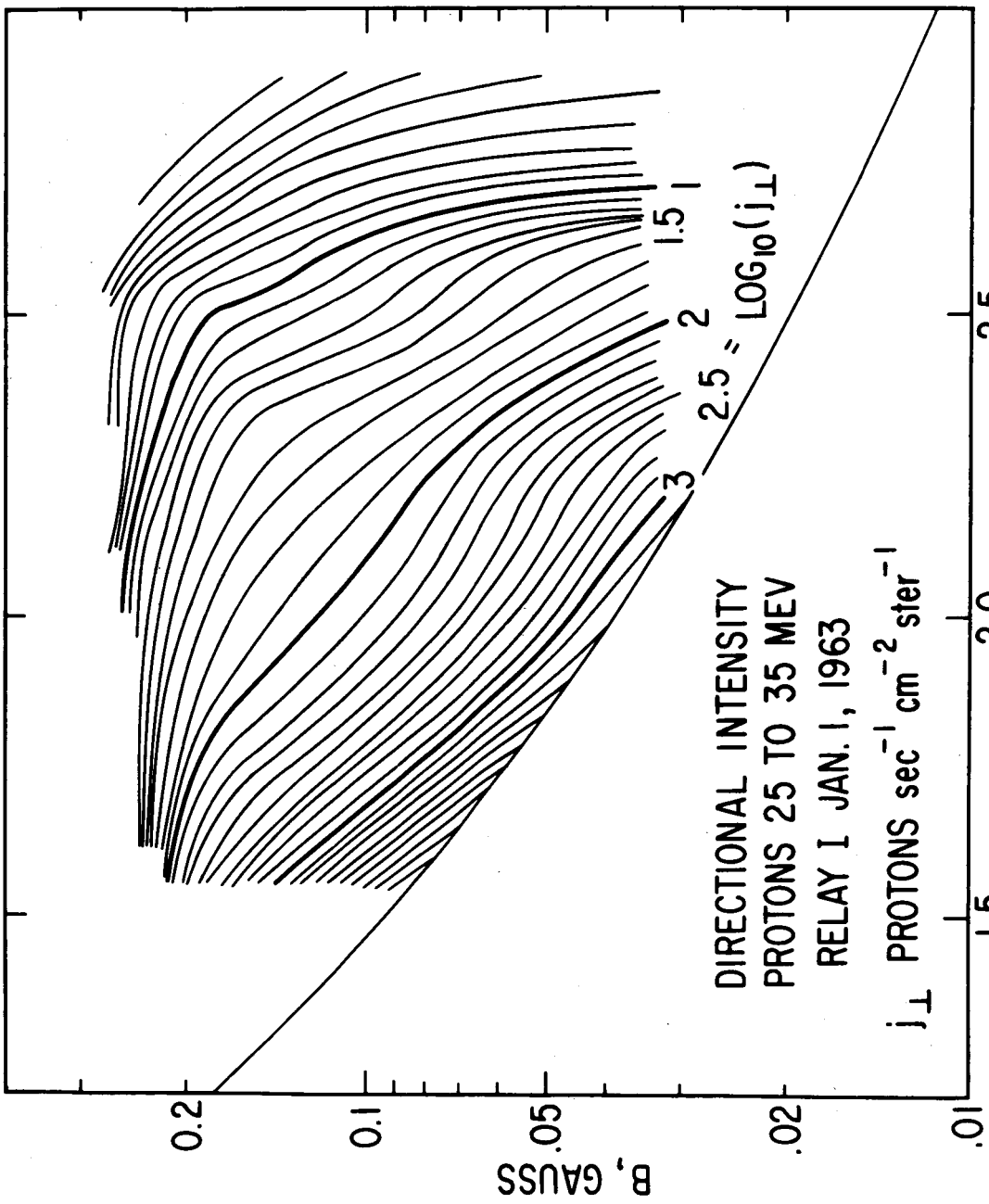
DIRECTIONAL INTENSITY
PROTONS 25 TO 35 MEV
RELAY I JAN. I, 1963
$j_\perp$ PROTONS $sec^{-1}\ cm^{-2}\ ster^{-1}$
$2.5 = LOG_{10}(j_\perp)$
3
2
1.5
1
B, GAUSS
0.2
0.1
.05
.02
.01
1.5
2.0
2.5
L, EARTH RADII

Figure 13

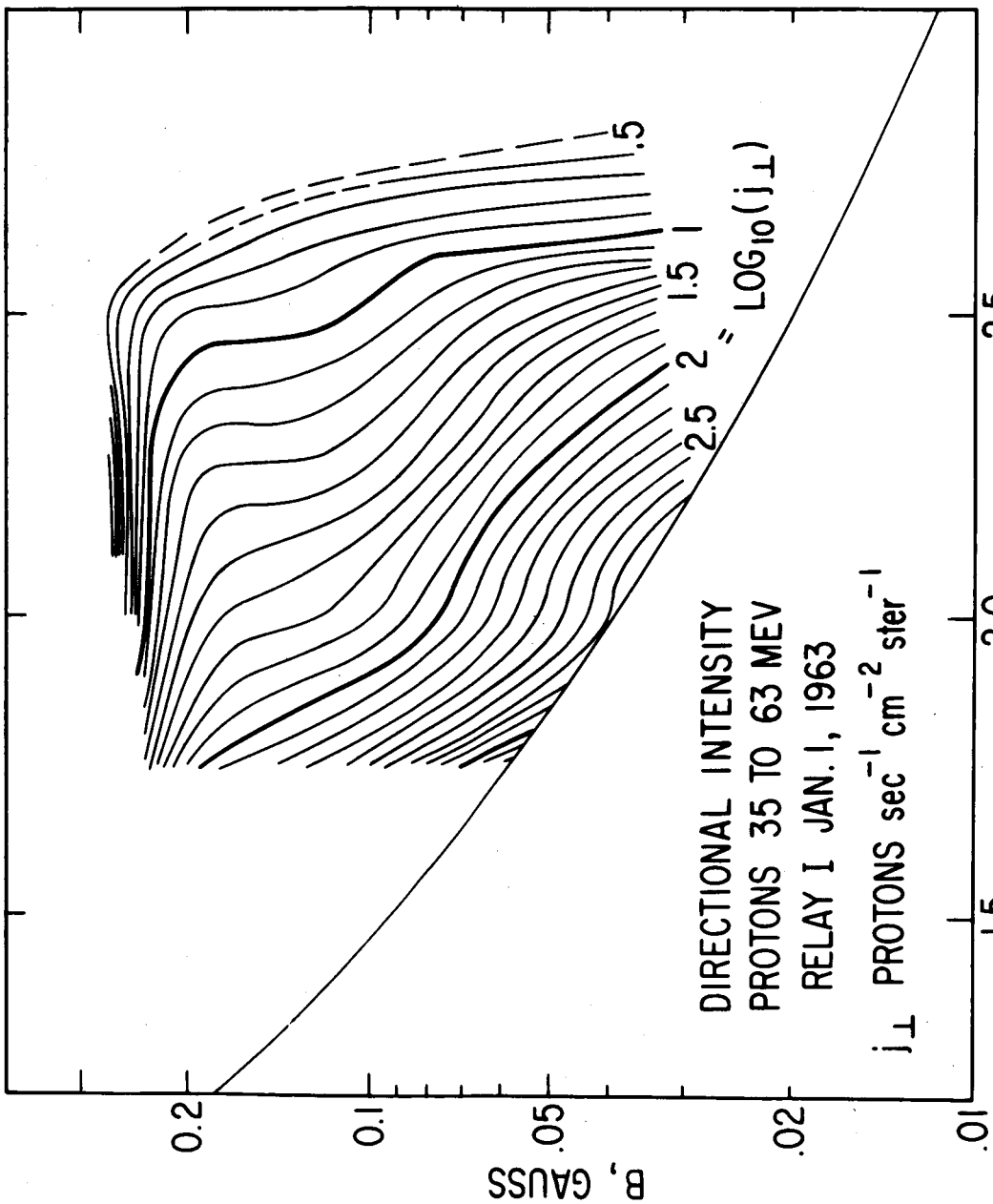
DIRECTIONAL INTENSITY
PROTONS 35 TO 63 MEV
RELAY I JAN. 1, 1963
$j_\perp$ PROTONS $sec^{-1} cm^{-2} ster^{-1}$
$= LOG_{10}(j_\perp)$
.5
1
1.5
2
2.5
B, GAUSS
.2
.1
.05
.02
.01
1.5
2.0
2.5
L, EARTH RADII

Figure 14

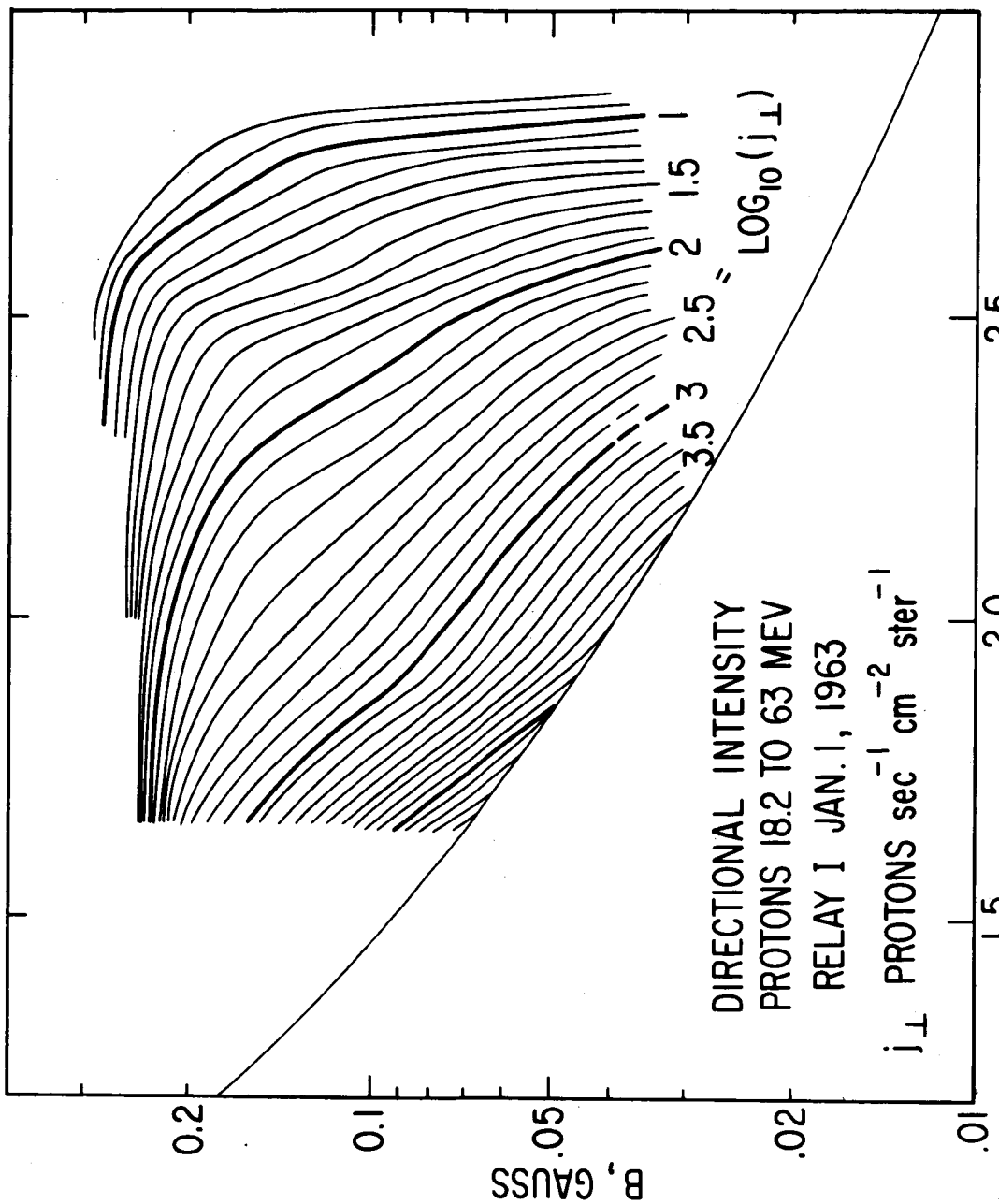
B, GAUSS
0.2
0.1
.05
.02
.01
1.5
2.0
2.5
L, EARTH RADII
DIRECTIONAL INTENSITY
PROTONS 18.2 TO 63 MEV
RELAY I JAN. 1, 1963
$j_\perp$ PROTONS sec^{-1} cm^{-2} $ster^{-1}$
$= LOG_{10}(j_\perp)$
1
1.5
2
2.5
3
3.5

Figure 15

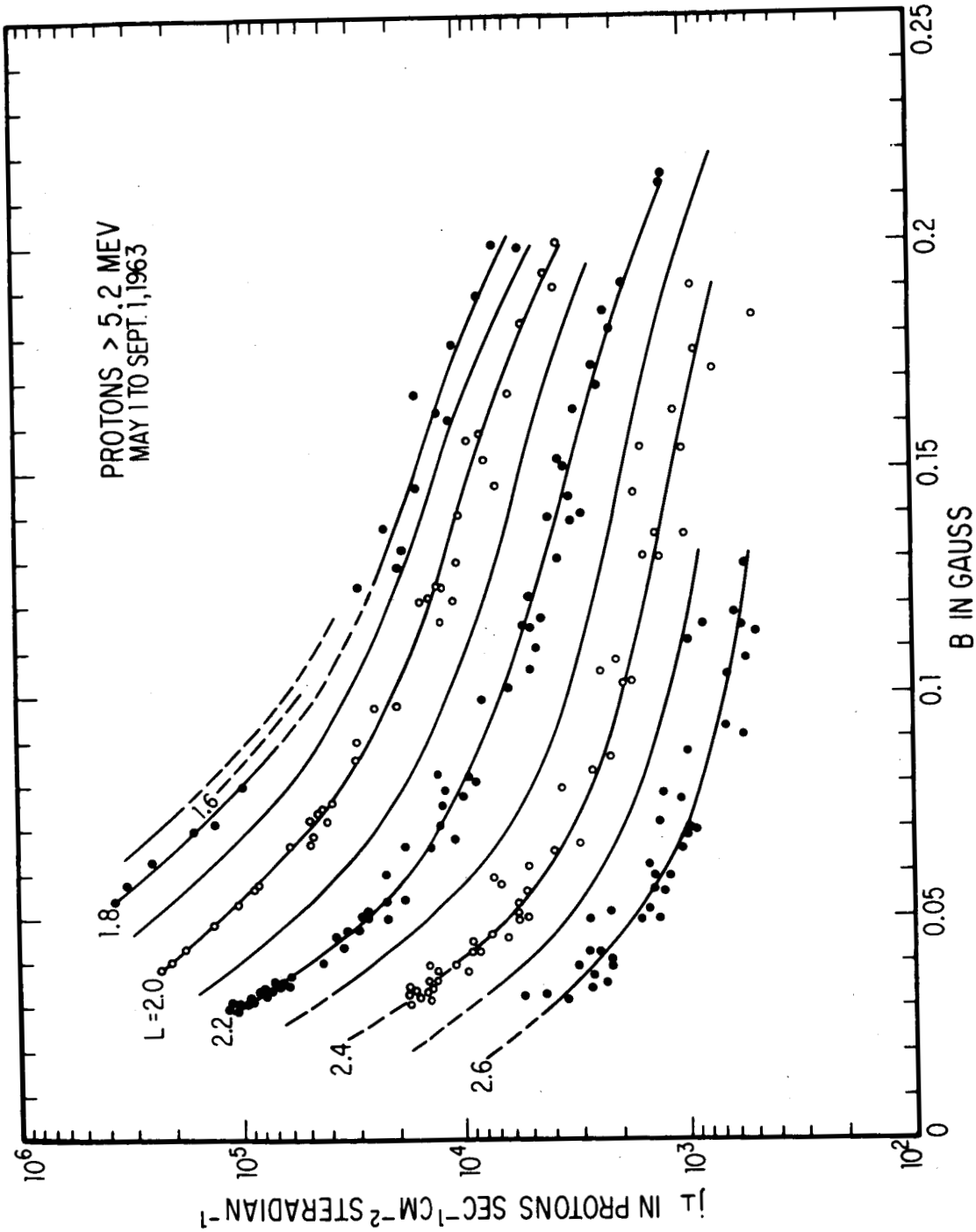
PROTONS > 5.2 MEV
MAY 1 TO SEPT. 1, 1963
1.8
1.6
L=2.0
2.2
2.4
2.6
B IN GAUSS
0
0.05
0.1
0.15
0.2
0.25
10^2
10^3
10^4
10^5
10^6
$j_\perp$ IN PROTONS $SEC^{-1}CM^{-2}$ STERADIAN^{-1}

Figure 16

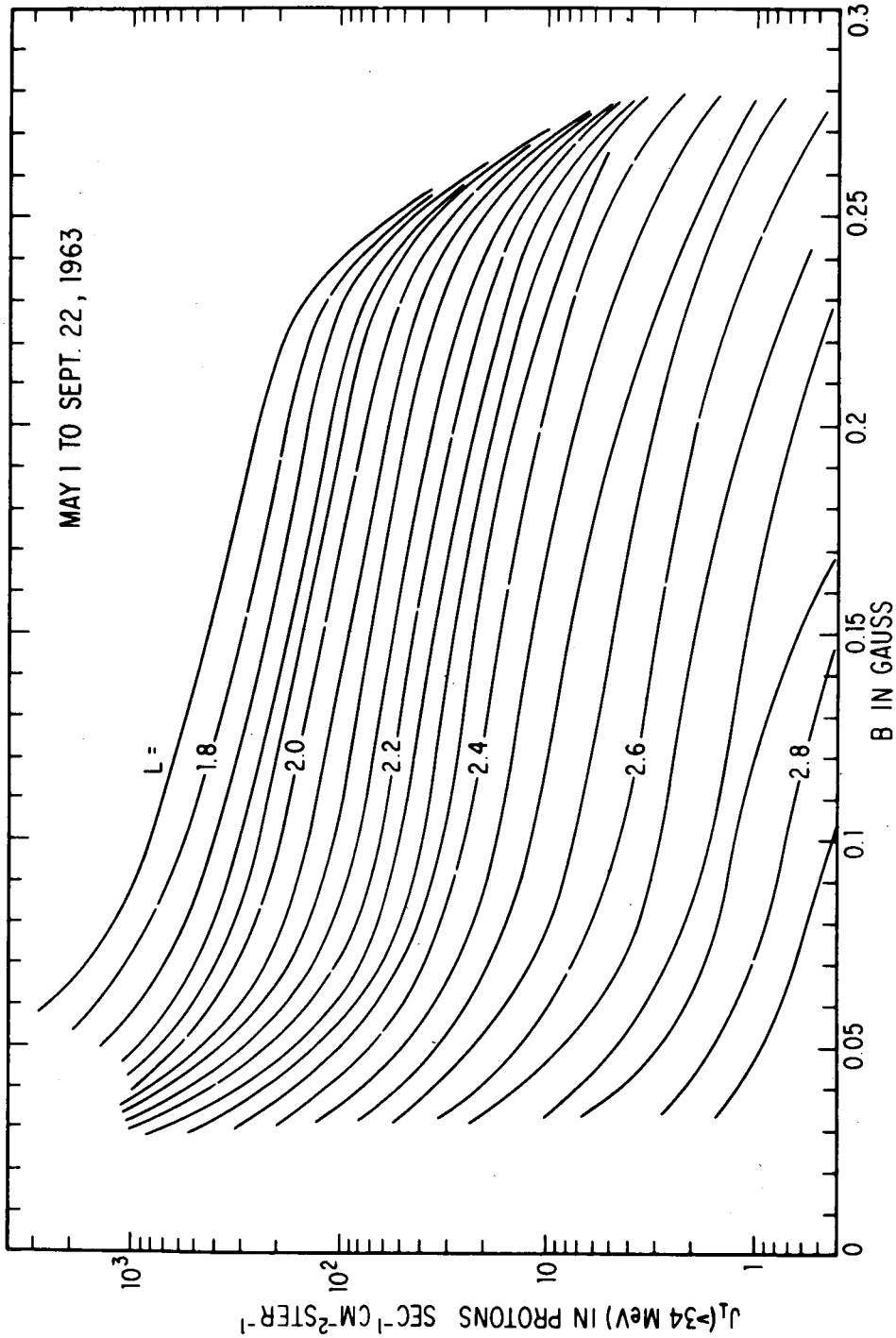
MAY 1 TO SEPT. 22, 1963
L=
1.8
2.0
2.2
2.4
2.6
2.8
10^3
10^2
10
1
0
0.05
0.1
0.15
0.2
0.25
0.3
B IN GAUSS
J_L(>34 MeV) IN PROTONS SEC^{-1} CM^{-2}STER^{-1}

Figure 17

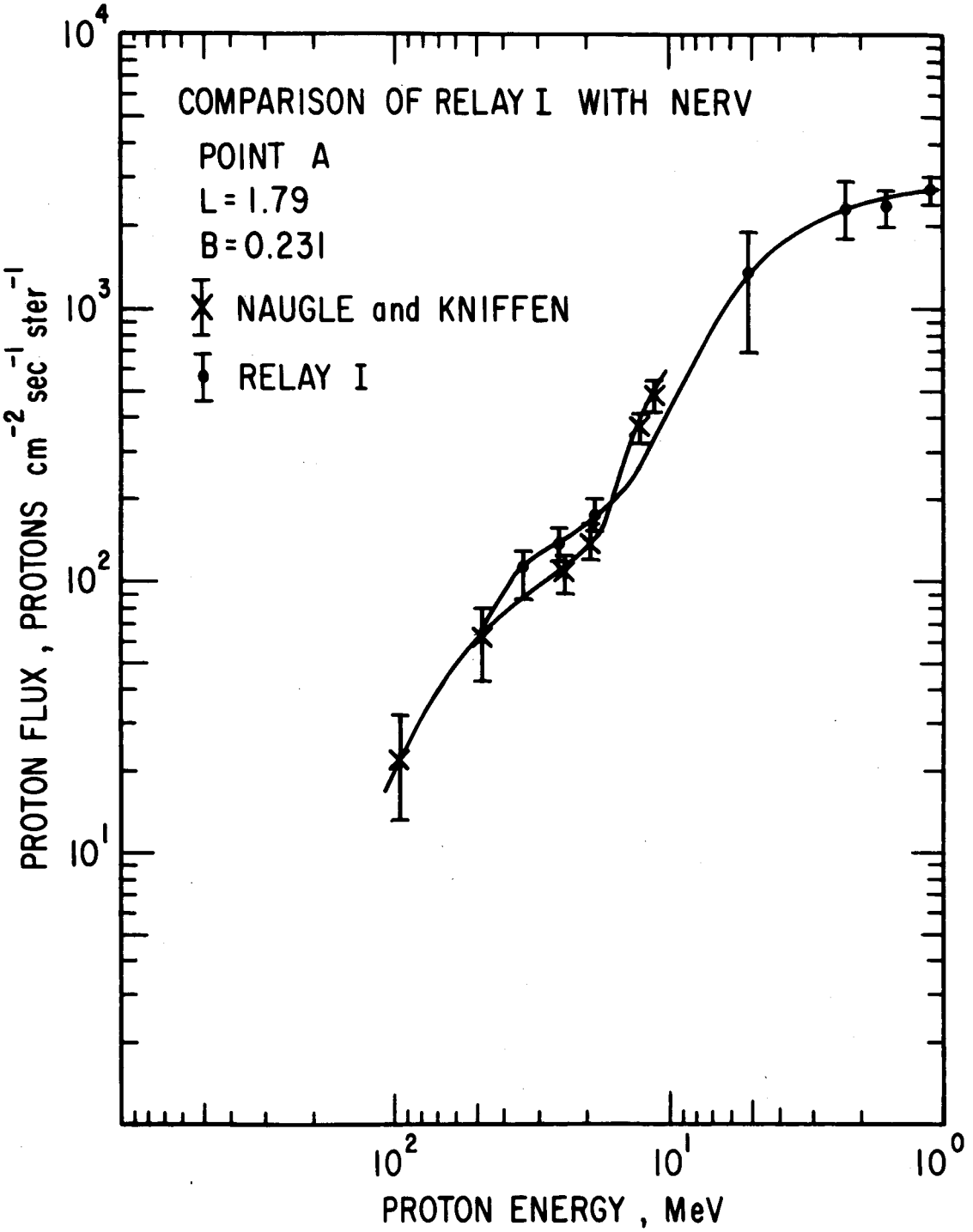
COMPARISON OF RELAY I WITH NERV
POINT A
L = 1.79
B = 0.231
NAUGLE and KNIFFEN
RELAY I
PROTON FLUX , PROTONS cm^{-2} sec^{-1} ster^{-1}
10^4
10^3
10^2
10^1
10^2
10^1
10^0
PROTON ENERGY , MeV

Figure 18

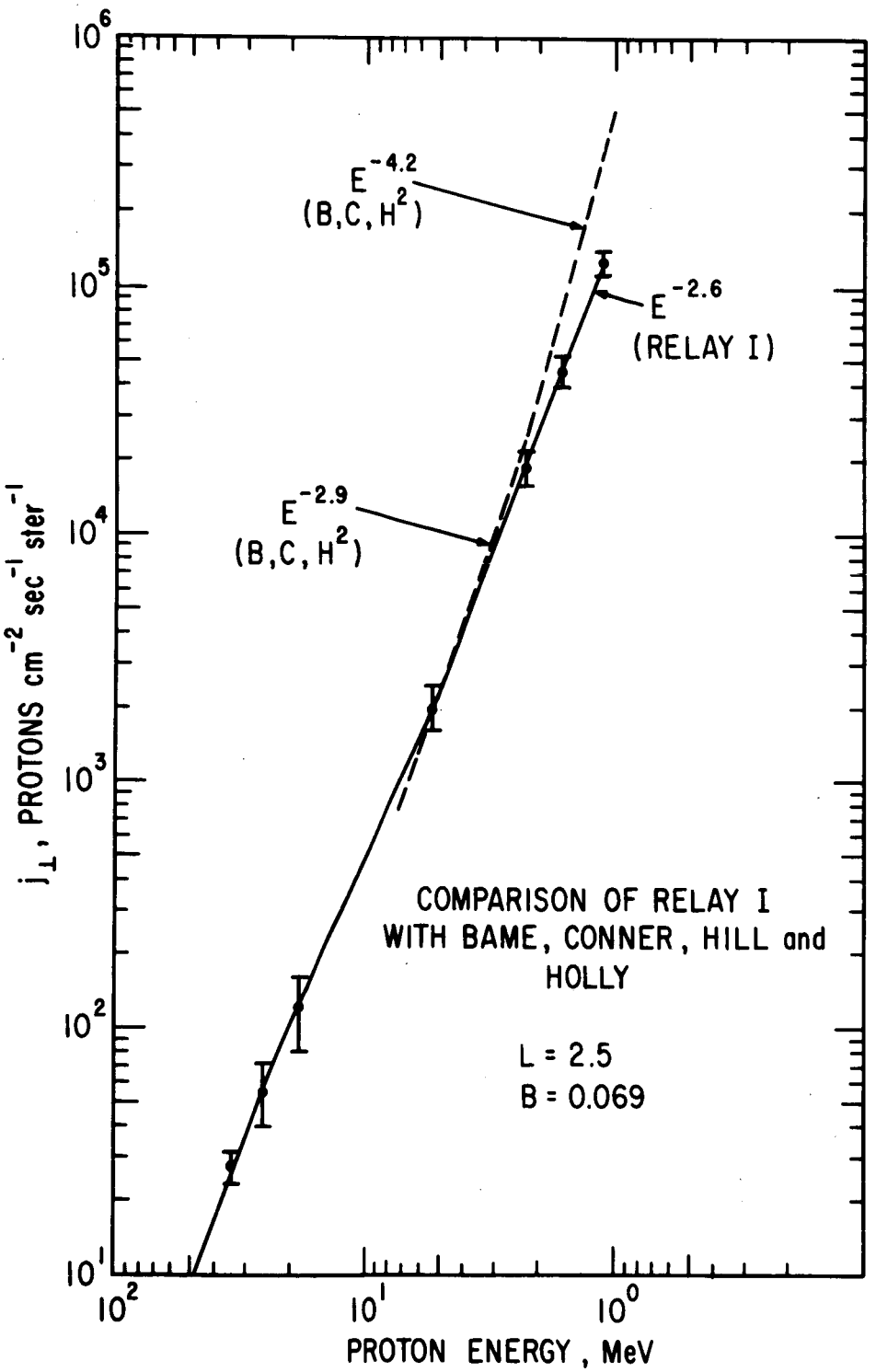
10^6
10^5
10^4
10^3
10^2
10^1
$E^{-4.2}$
(B,C,H^2)
$E^{-2.6}$
(RELAY I)
$E^{-2.9}$
(B,C,H^2)
COMPARISON OF RELAY I
WITH BAME, CONNER, HILL and
HOLLY
L = 2.5
B = 0.069
$j_\perp$, PROTONS cm^{-2} sec^{-1} $ster^{-1}$
10^2
10^1
10^0
PROTON ENERGY, MeV

Figure 19

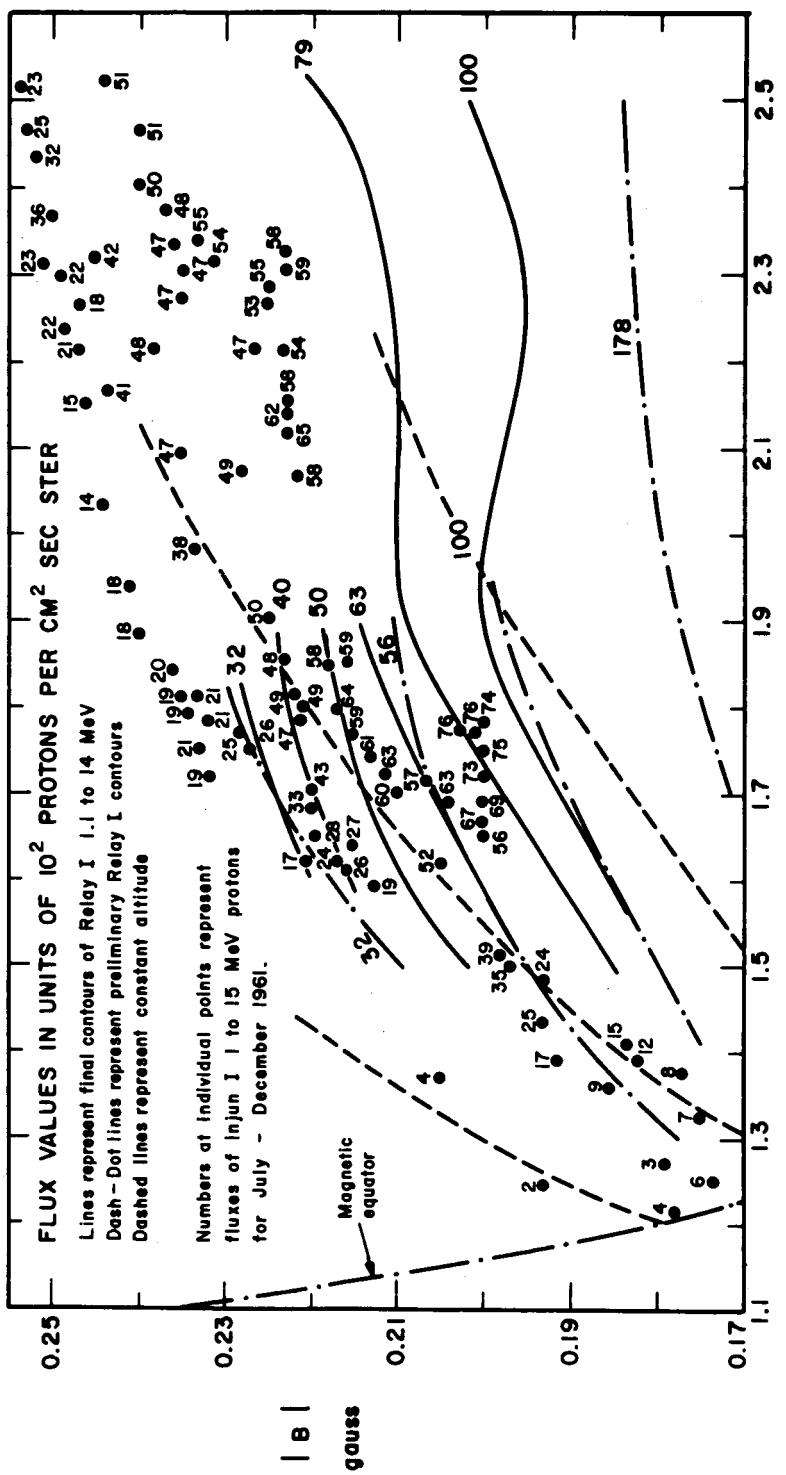
FLUX VALUES IN UNITS OF 10^2 PROTONS PER CM^2 SEC STER
Lines represent final contours of Relay I 1.1 to 14 MeV
Dash – Dot lines represent preliminary Relay I contours
Dashed lines represent constant altitude
Numbers at individual points represent fluxes of Injun I 1 to 15 MeV protons for July – December 1961.
Magnetic equator
|B| gauss
L, earth radii
0.25
0.23
0.21
0.19
0.17
1.1
1.3
1.5
1.7
1.9
2.1
2.3
2.5
79
100
100
178

Figure 20

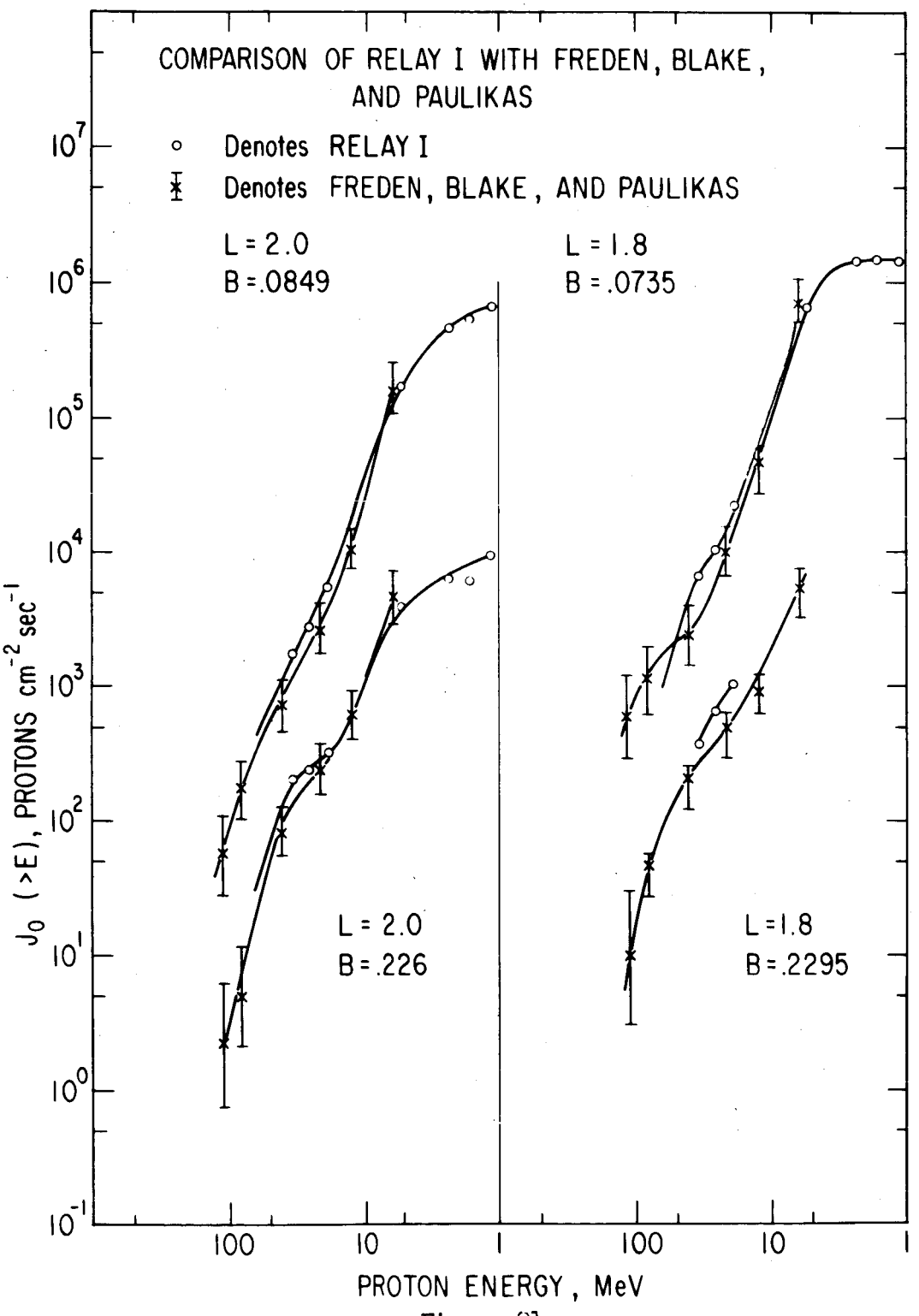
COMPARISON OF RELAY I WITH FREDEN, BLAKE, AND PAULIKAS
Denotes RELAY I
Denotes FREDEN, BLAKE, AND PAULIKAS
L = 2.0
B = .0849
L = 1.8
B = .0735
L = 2.0
B = .226
L = 1.8
B = .2295
J_0 (>E), PROTONS cm^{-2} sec^{-1}
10^7
10^6
10^5
10^4
10^3
10^2
10^1
10^0
10^{-1}
100
10
1
100
10
1
PROTON ENERGY, MeV

Figure 21

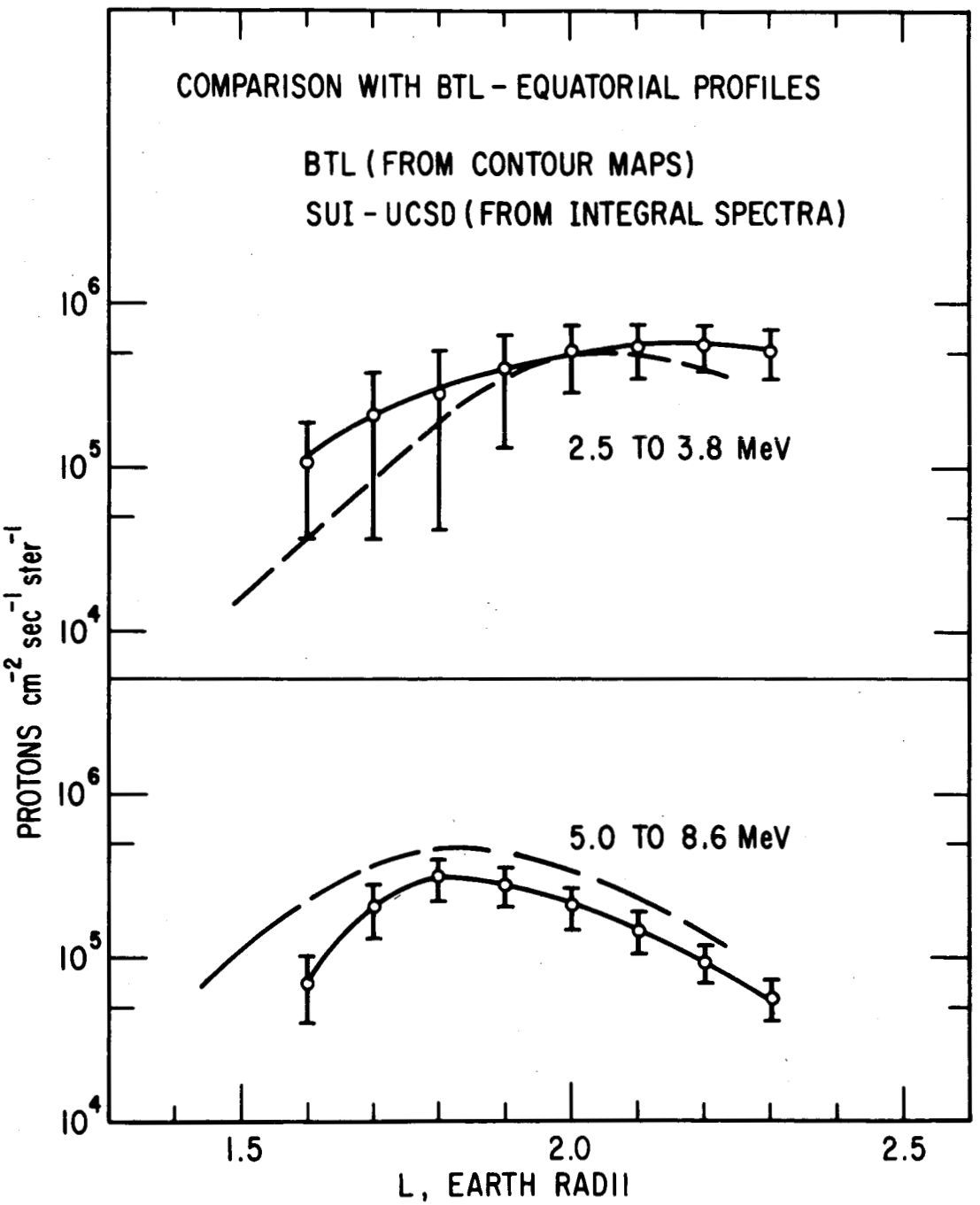
COMPARISON WITH BTL - EQUATORIAL PROFILES
BTL (FROM CONTOUR MAPS)
SUI - UCSD (FROM INTEGRAL SPECTRA)
2.5 TO 3.8 MeV
5.0 TO 8.6 MeV
PROTONS cm^{-2} sec^{-1} ster^{-1}
10^6
10^5
10^4
1.5
2.0
2.5
L, EARTH RADII

Figure 22

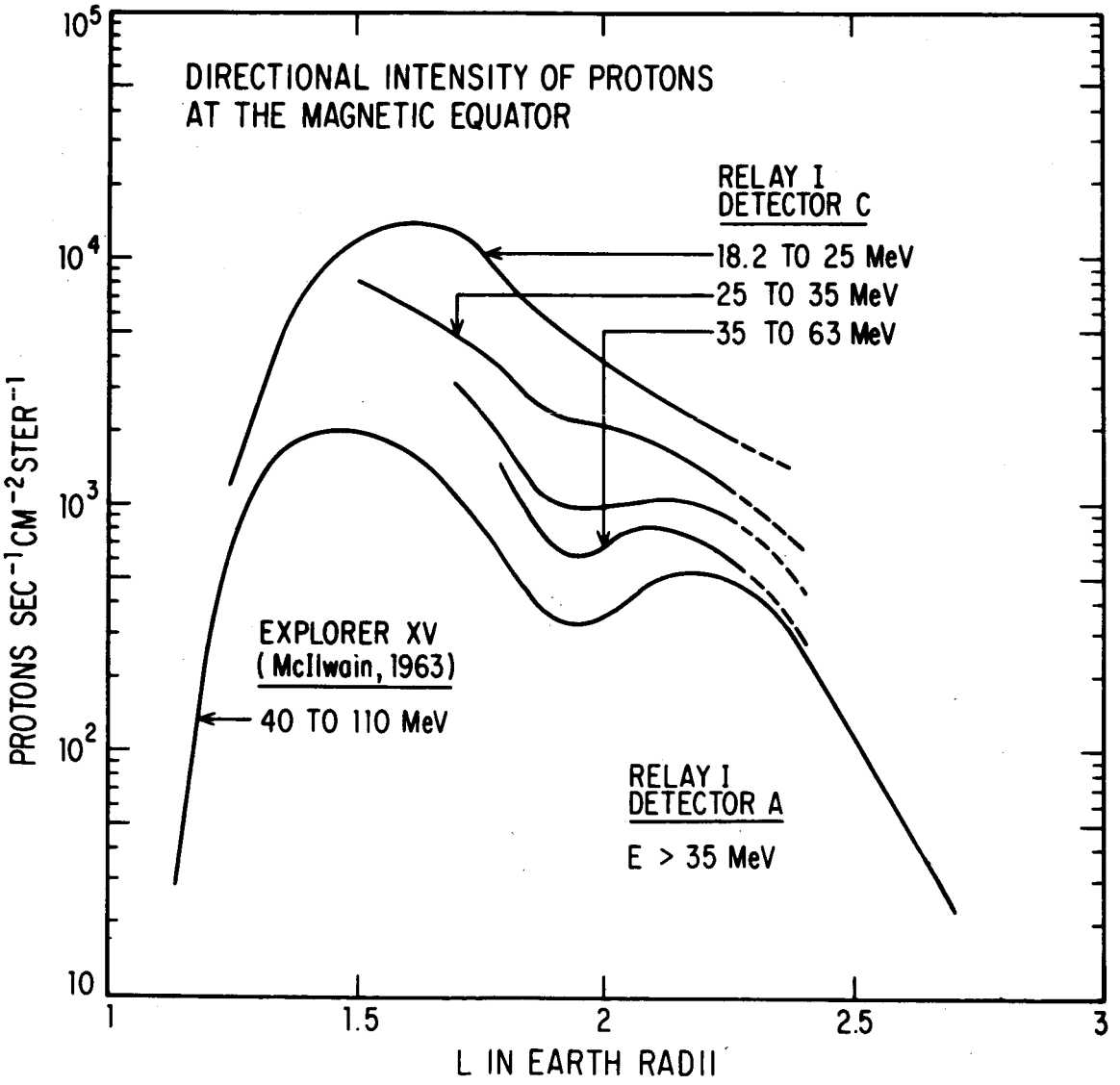
DIRECTIONAL INTENSITY OF PROTONS
AT THE MAGNETIC EQUATOR
RELAY I
DETECTOR C
18.2 TO 25 MeV
25 TO 35 MeV
35 TO 63 MeV
EXPLORER XV
(McIlwain, 1963)
40 TO 110 MeV
RELAY I
DETECTOR A
E > 35 MeV
PROTONS SEC^{-1}CM^{-2}STER^{-1}
L IN EARTH RADII
10^5
10^4
10^3
10^2
10
1
1.5
2
2.5
3

Figure 23

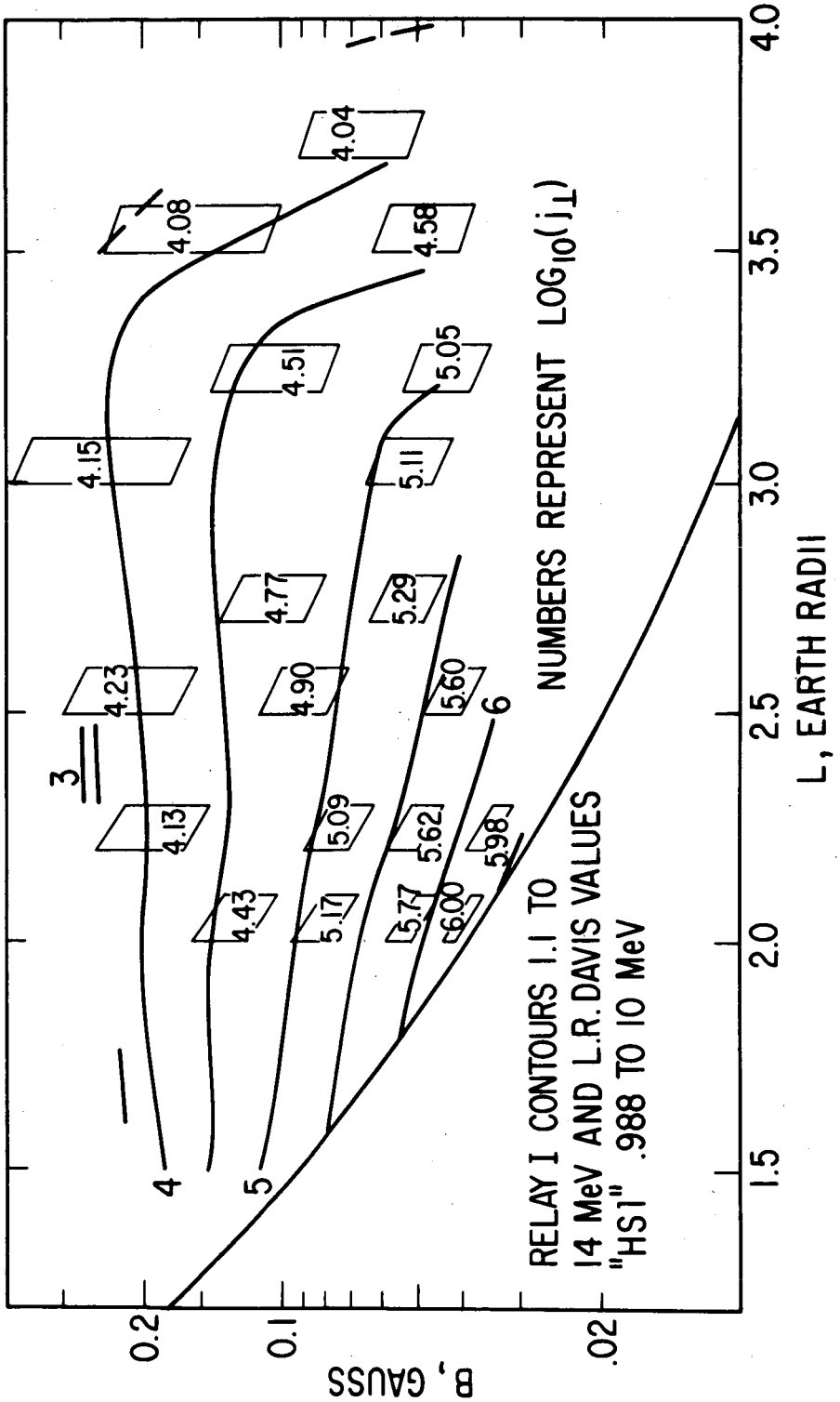
RELAY I CONTOURS 1.1 TO
14 MeV AND L.R. DAVIS VALUES
"HS1" .988 TO 10 MeV
NUMBERS REPRESENT LOG10(j⊥)
B, GAUSS
L, EARTH RADII
0.2
0.1
.02
1.5
2.0
2.5
3.0
3.5
4.0
4
5
6
3
4.04
4.08
4.58
4.51
5.05
4.15
5.11
4.77
5.29
4.23
4.90
5.60
4.13
5.09
5.62
5.98
4.43
5.17
5.77
6.00

Figure 24

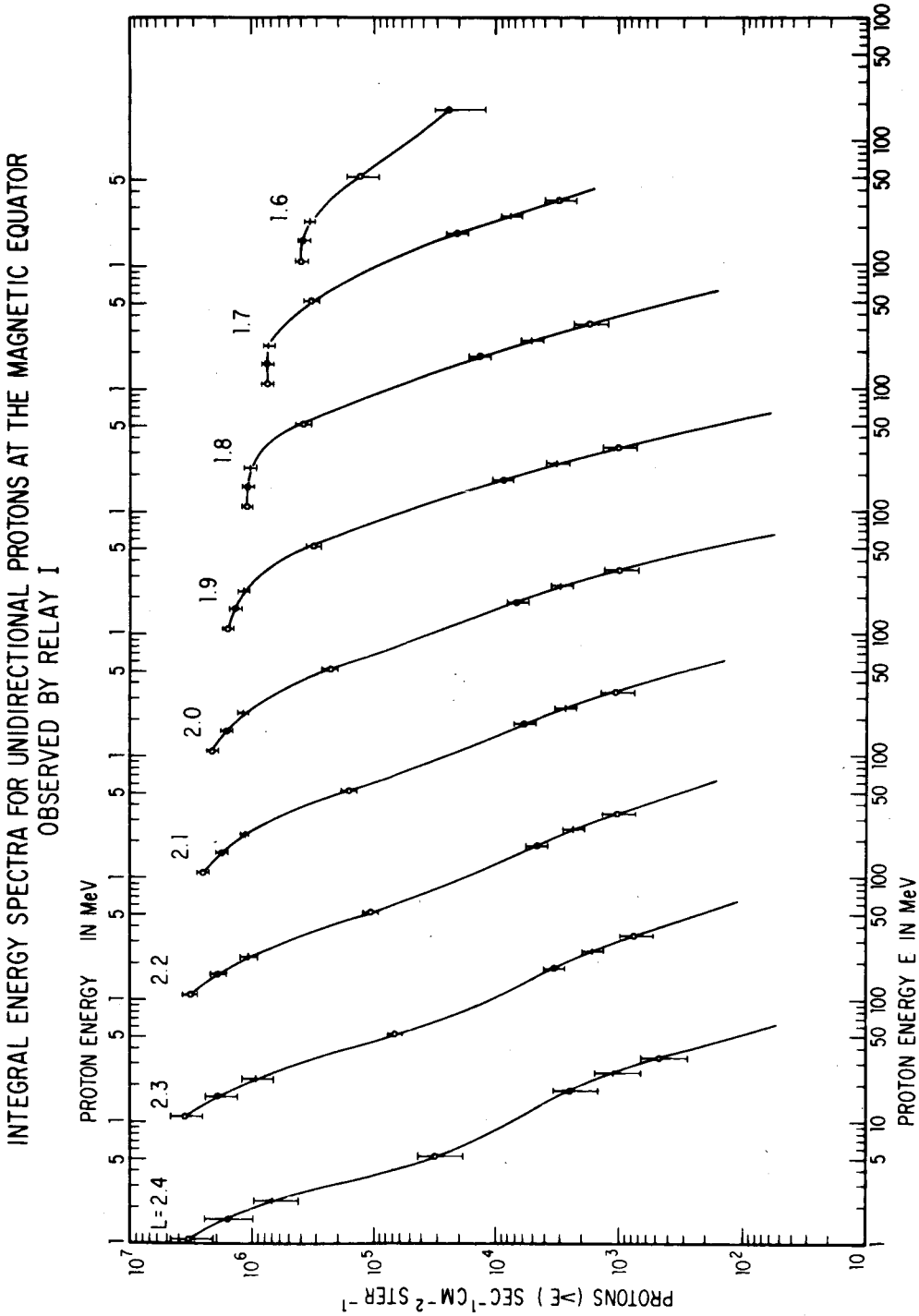
INTEGRAL ENERGY SPECTRA FOR UNIDIRECTIONAL PROTONS AT THE MAGNETIC EQUATOR
OBSERVED BY RELAY I
PROTON ENERGY IN MeV
PROTONS (>E) SEC⁻¹CM⁻²STER⁻¹
PROTON ENERGY E IN MeV
L=2.4
2.3
2.2
2.1
2.0
1.9
1.8
1.7
1.6

Figure 25

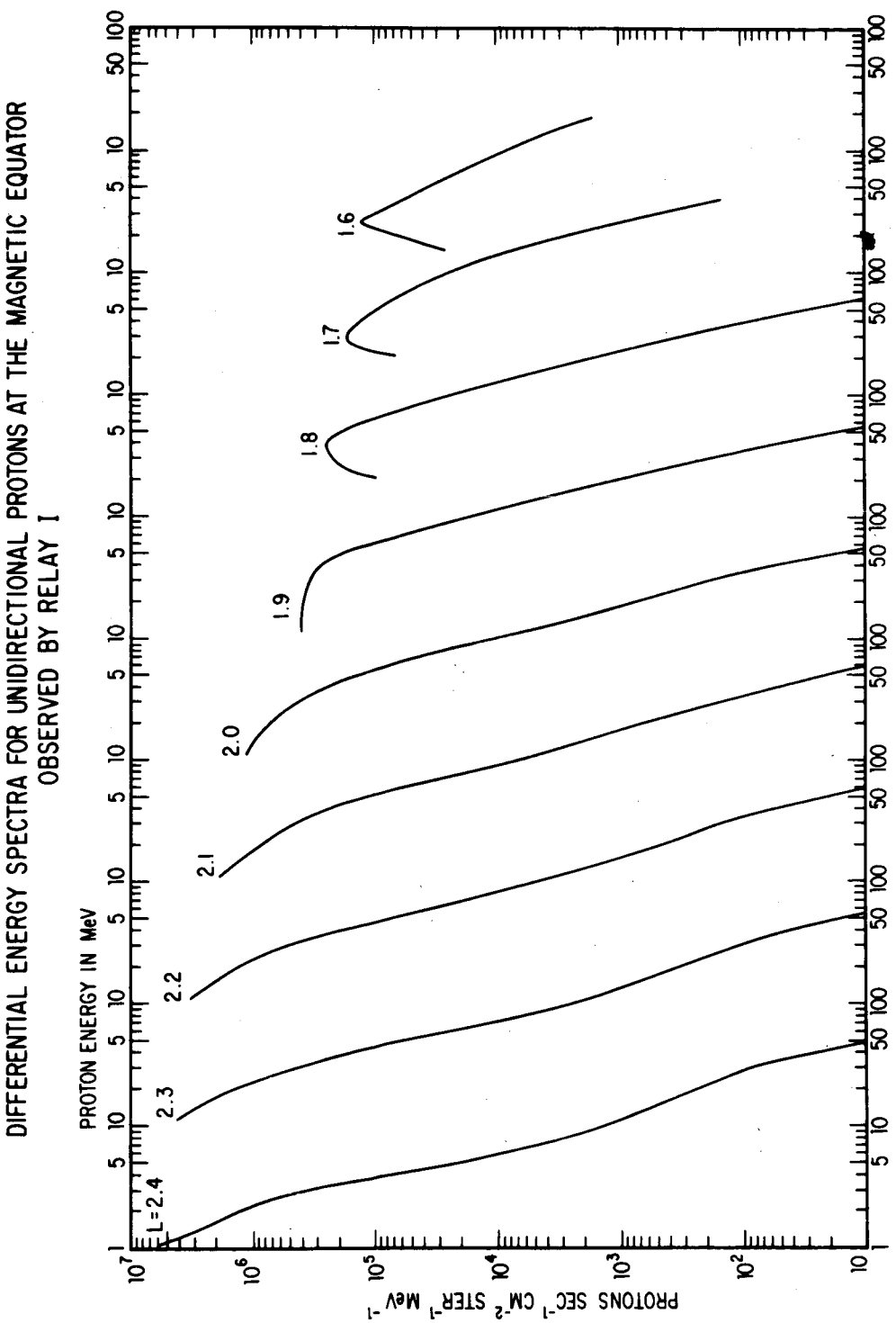
DIFFERENTIAL ENERGY SPECTRA FOR UNIDIRECTIONAL PROTONS AT THE MAGNETIC EQUATOR
OBSERVED BY RELAY I
PROTON ENERGY IN MeV
PROTONS SEC⁻¹ CM⁻² STER⁻¹ MeV⁻¹
L=2.4
2.3
2.2
2.1
2.0
1.9
1.8
1.7
1.6

Figure 26

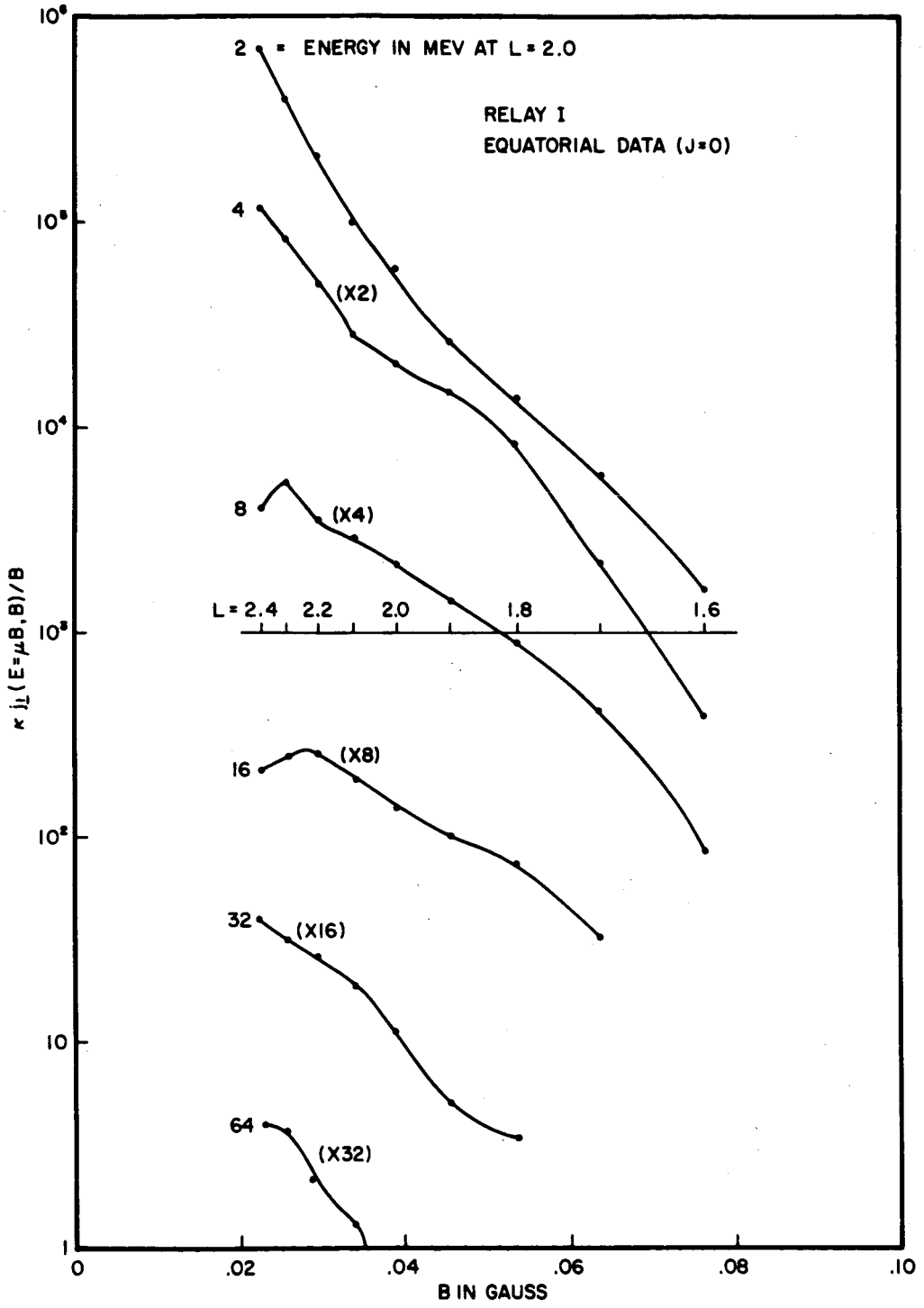
2 = ENERGY IN MEV AT L = 2.0
RELAY I
EQUATORIAL DATA (J=0)
4
(X2)
8
(X4)
L = 2.4 2.2 2.0 1.8 1.6
16
(X8)
32
(X16)
64
(X32)
κ j_L (E=μB, B)/B
B IN GAUSS
0
.02
.04
.06
.08
.10
1
10
10²
10³
10⁴
10⁵
10⁶

Figure 27

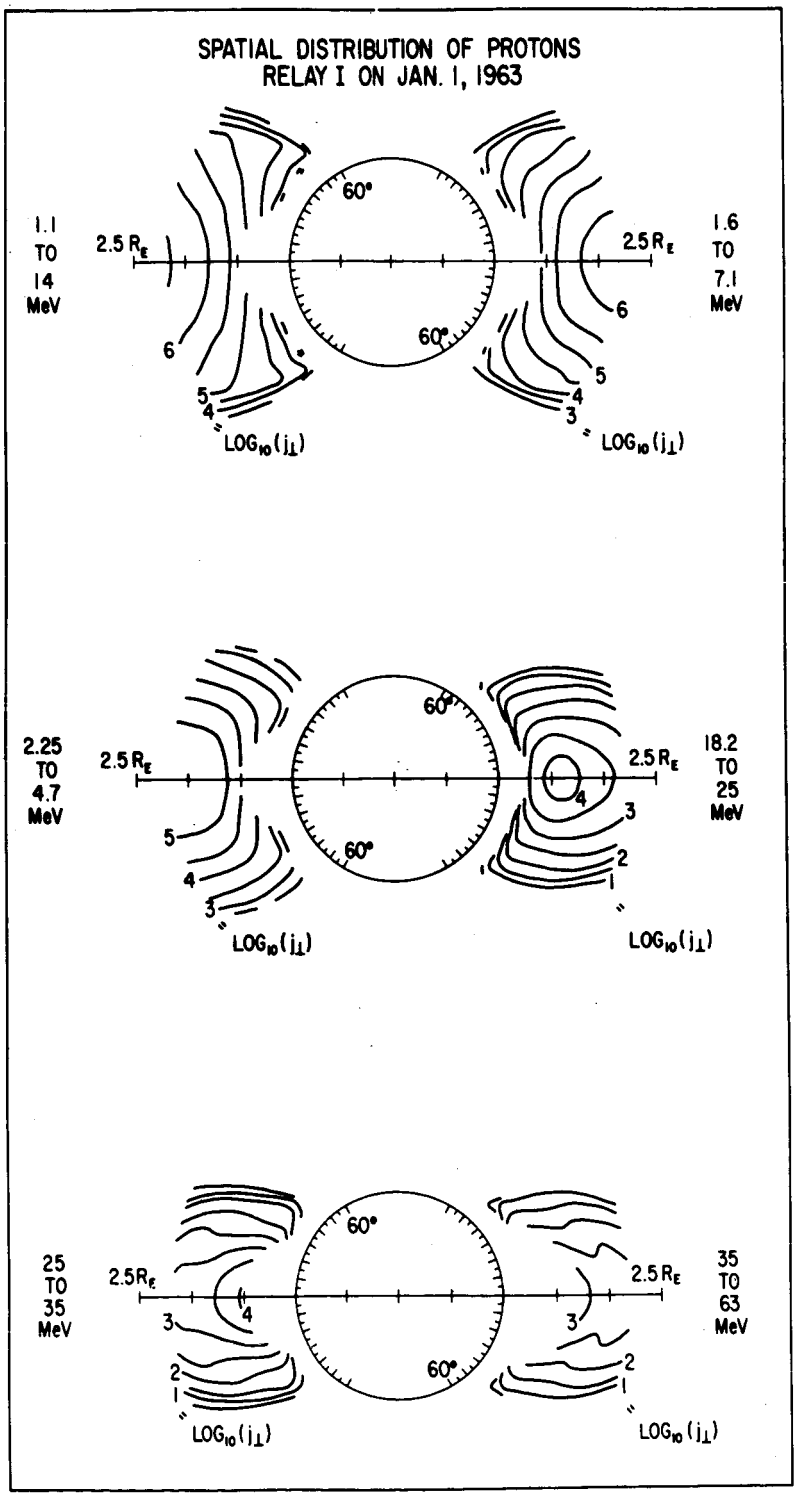
SPATIAL DISTRIBUTION OF PROTONS
RELAY I ON JAN. 1, 1963
1.1 TO 14 MeV
1.6 TO 7.1 MeV
2.25 TO 4.7 MeV
18.2 TO 25 MeV
25 TO 35 MeV
35 TO 63 MeV
2.5 R_E
60°
LOG10(j⊥)

Figure 28

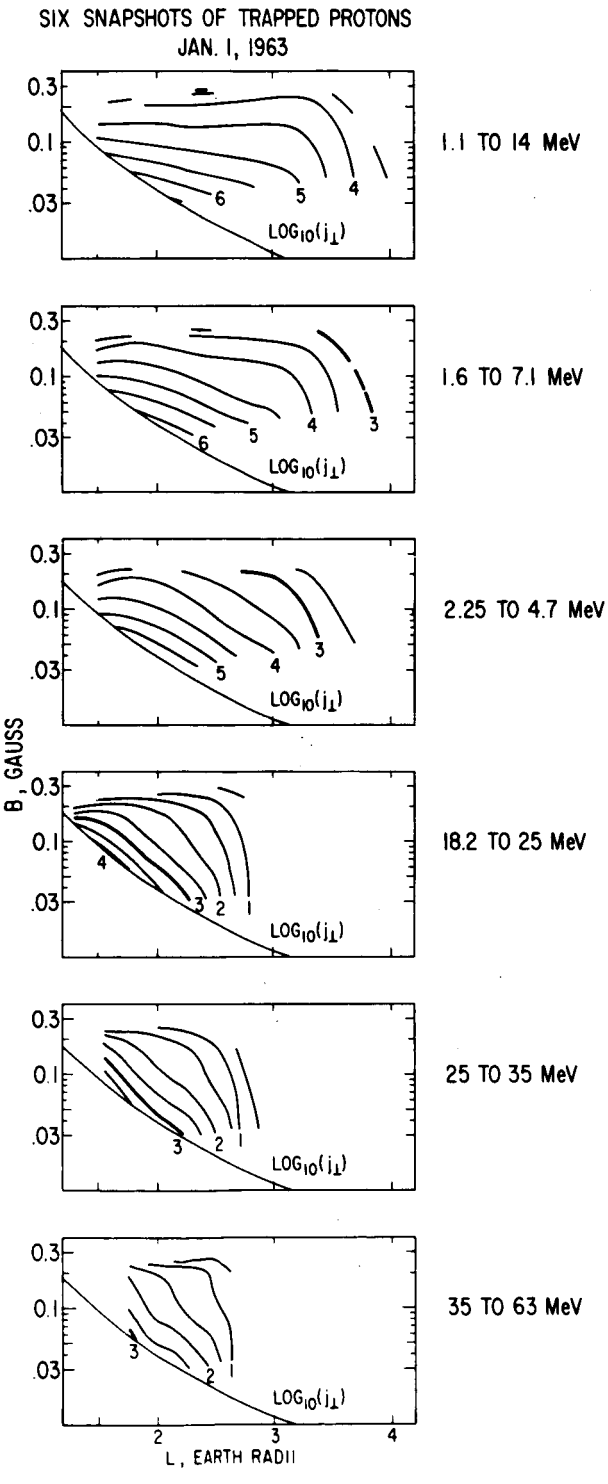
SIX SNAPSHOTS OF TRAPPED PROTONS
JAN. 1, 1963
B, GAUSS
L, EARTH RADII
LOG10(j⊥)
1.1 TO 14 MeV
1.6 TO 7.1 MeV
2.25 TO 4.7 MeV
18.2 TO 25 MeV
25 TO 35 MeV
35 TO 63 MeV

Figure 29

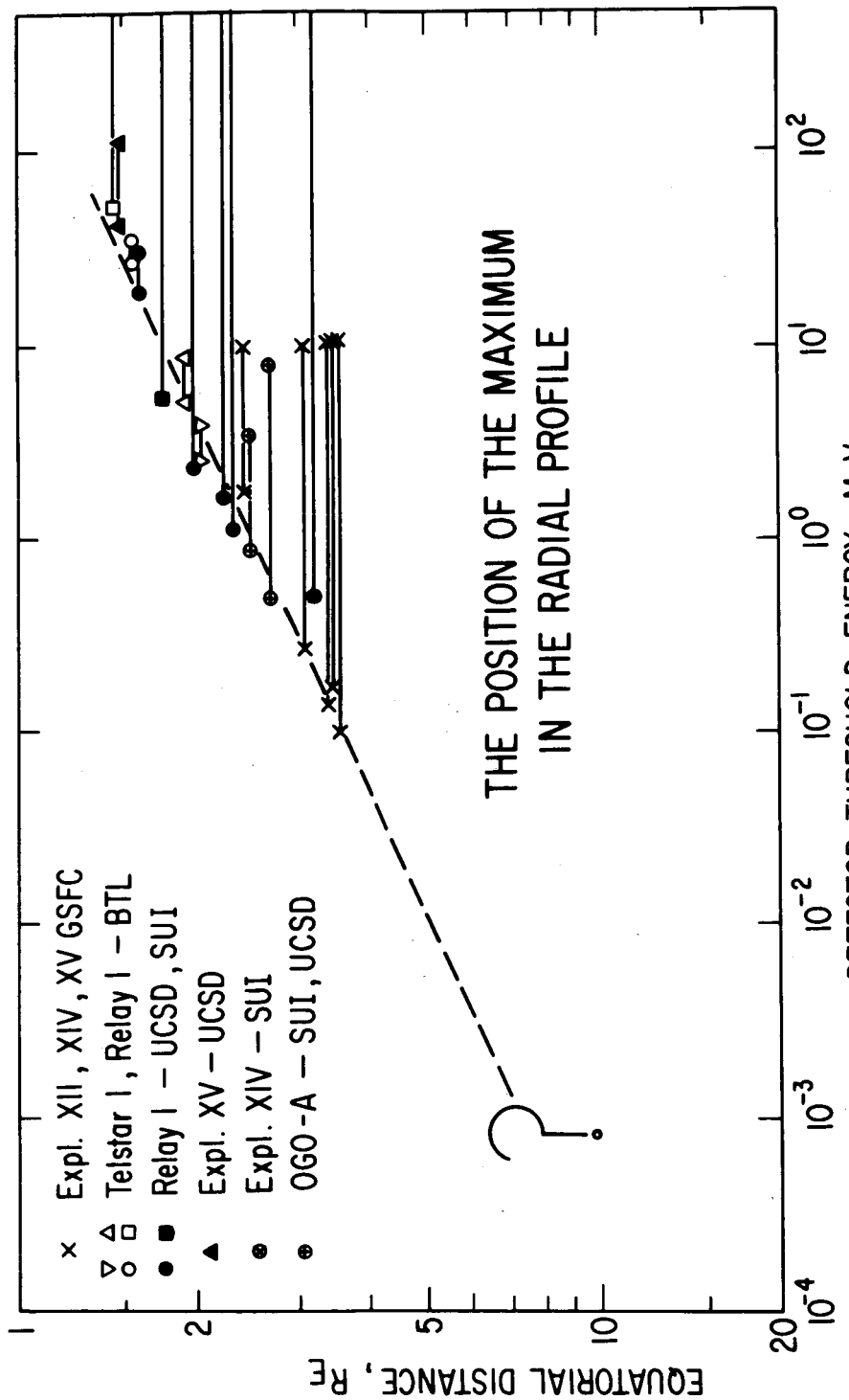
EQUATORIAL DISTANCE, R_E
DETECTOR THRESHOLD ENERGY, MeV
THE POSITION OF THE MAXIMUM
IN THE RADIAL PROFILE
Expl. XII, XIV, XV GSFC
Telstar I, Relay I – BTL
Relay I – UCSD, SUI
Expl. XV – UCSD
Expl. XIV – SUI
OGO-A – SUI, UCSD

Figure 30

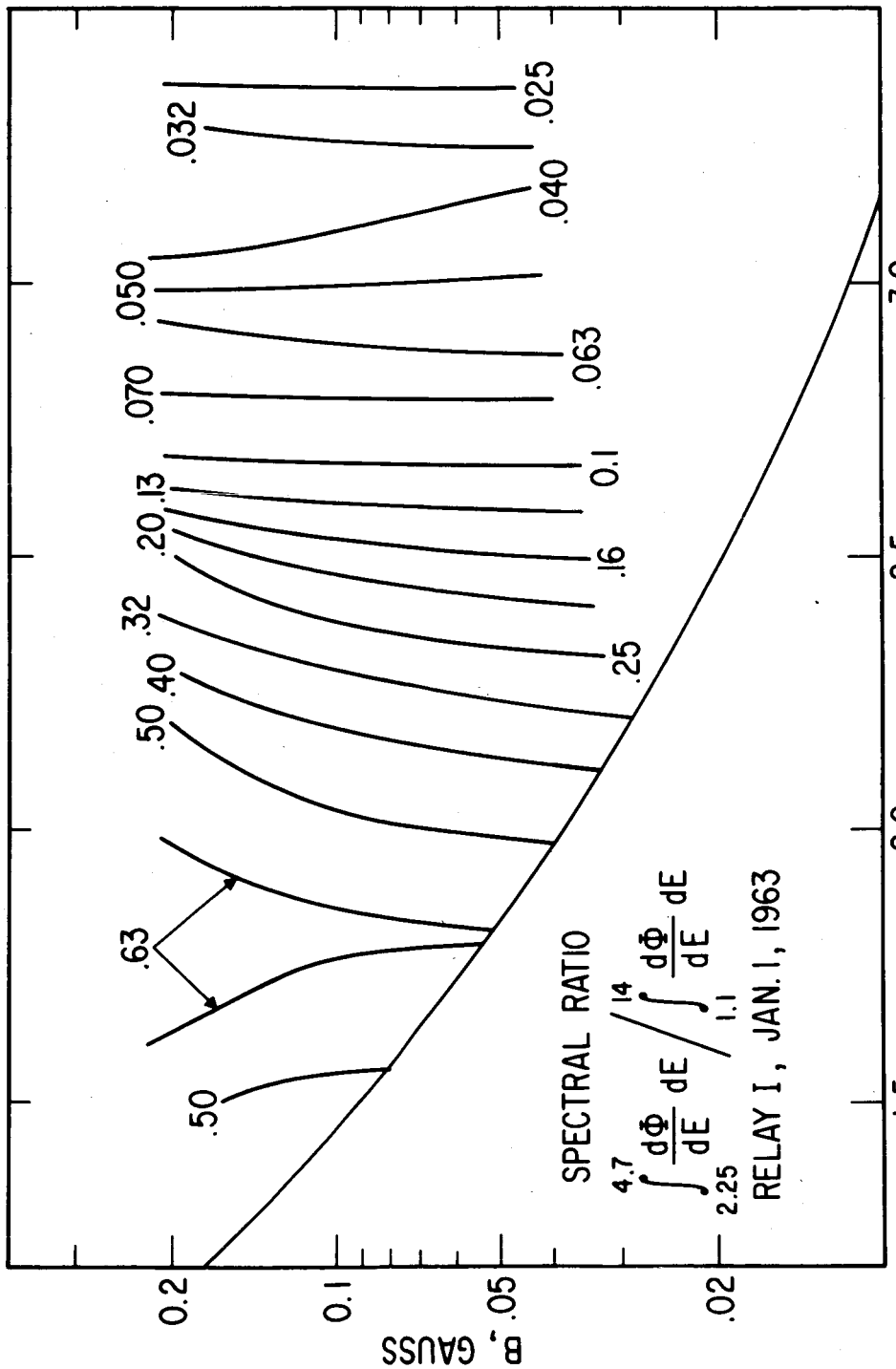
B, GAUSS
0.2
0.1
.05
.02
1.5
2.0
2.5
3.0
L IN EARTH RADII
.025
.032
.040
.050
.063
.070
0.1
.13
.16
.20
.25
.32
.40
.50
.63
.50
SPECTRAL RATIO
$\int_{2.25}^{4.7} \frac{d\Phi}{dE} dE \Big/ \int_{1.1}^{14} \frac{d\Phi}{dE} dE$
RELAY I, JAN. 1, 1963

Figure 31

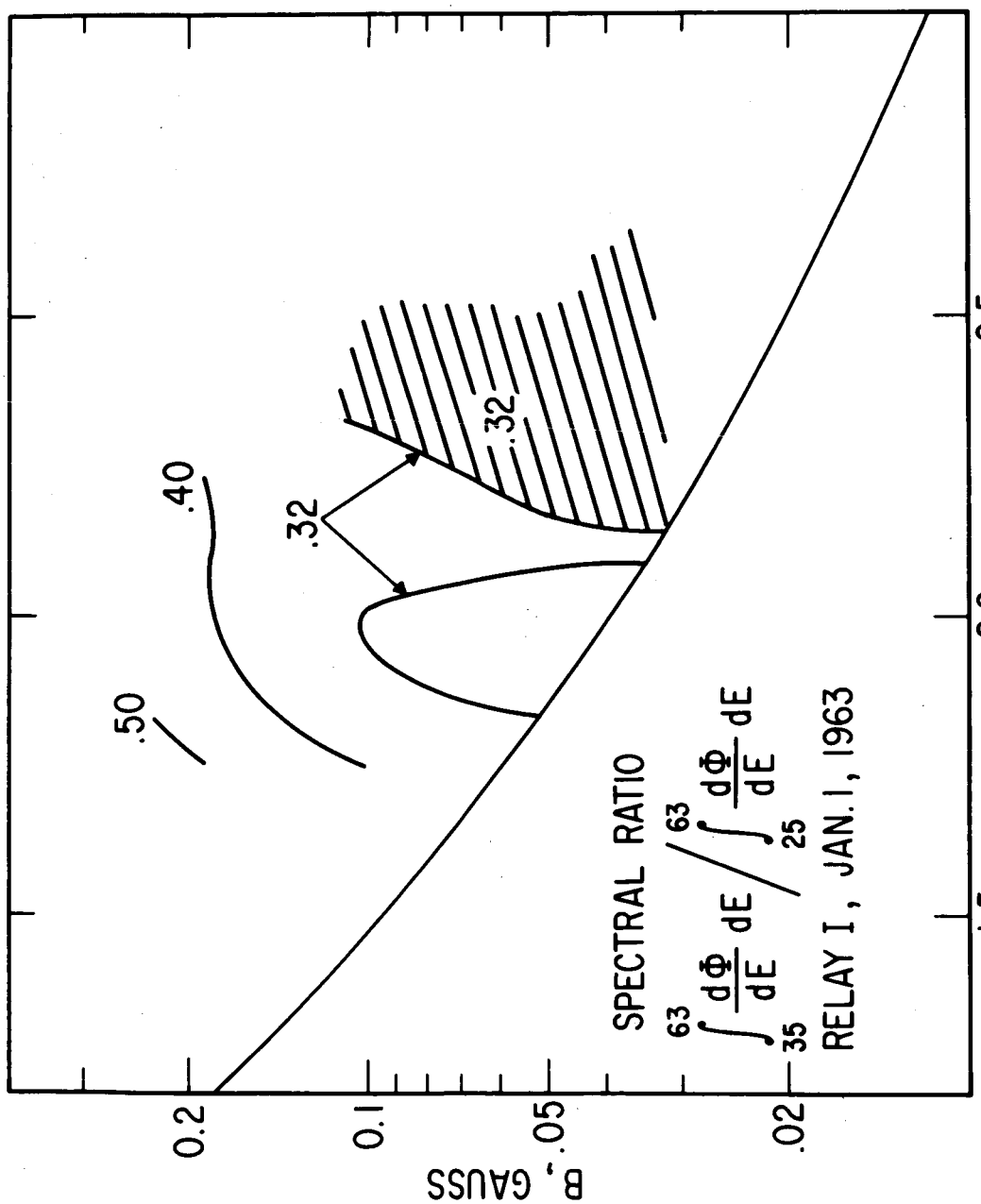
B, GAUSS
0.2
0.1
.05
.02
1.5
2.0
2.5
L IN EARTH RADII
.50
.40
.32
.32
SPECTRAL RATIO
$\int_{35}^{63} \frac{d\Phi}{dE} dE \Big/ \int_{25}^{63} \frac{d\Phi}{dE} dE$
RELAY I, JAN. 1, 1963

Figure 32